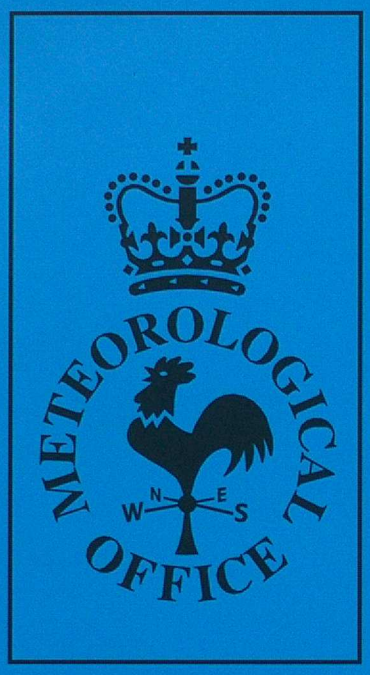

Forecasting Research

Forecasting Research Division
Technical Report No. 202

Evaluation of the Use of SSM/I Data and a Microphysical Model to Establish an Aircraft Icing Environment

by

R Brown and G Holpin

October 1996

Meteorological Office
London Road
Bracknell
Berkshire
RG12 2SZ
United Kingdom

Forecasting Research
Technical Report No. 202

Evaluation of the Use of SSM/I Data and a Microphysical Model to Establish an Aircraft Icing Environment

by

R Brown and G Holpin

October 1996

Forecasting Research
Meteorological Office
London Road
Bracknell
Berkshire
RG12 2SZ
United Kingdom

Evaluation of the Use of SSM/I Data and a Microphysical Model to Establish an Aircraft Icing Environment

R. Brown and G. Holpin
Meteorological Office
October 1996

1. Introduction

The current aircraft icing environment, as contained in FAA 25, JAA 25 Appendix C, describes the occurrence of supercooled liquid water and associated drop sizes as a function of temperature. The region of the height-temperature domain where icing is likely is also described. The current icing environment is based on aircraft measurements made in the forties and fifties. Jeck (1983) has produced a similar climatology based upon more modern aircraft data, obtained from various locations, mainly in the United States and Europe. Lunnon (1993) has pointed out the limitations of these data. The air-borne instruments only sample an extremely small volume of air and data from a very limited number of geographical locations has been included.

Lunnon (1993) proposed that a new icing environment should be developed, based upon remotely-sensed data and model information. Remote sensing, particularly from satellite-borne instrumentation, has the advantage of sampling a large volume of the atmosphere and the potential to provide global coverage. The disadvantage when used to infer supercooled liquid water contents is that it is of relatively unknown accuracy compared to aircraft data.

This report describes the evaluation of one of the main techniques proposed by Lunnon (1993) which uses microwave measurements and a two-dimensional microphysical model to derive a new climatology of supercooled liquid water content (LWC). The methodology is described in Section 2 and initial attempts at validation in Section 3. Because serious problems were encountered, a variety of other investigations of the technique were undertaken and these are described in Sections 4 to 6. Conclusions drawn from these investigations are given in Section 7, the main one being that the technique requires a significant amount of further development before being employed as envisaged.

2. Methodology and Tools

2.1 Basic Method

The proposed technique uses microwave measurements from the Special Sensor Microwave Instrument (SSM/I) flown on the US Defence Meteorological Satellite Program (DMSP). The DMSP satellites are in sun-synchronous polar orbit. The SSM/I makes passive microwave measurements of brightness temperature at 4 frequencies. The spatial resolution varies from 69 x 43 km at 19 Ghz to 15 x 13 km at 85 Ghz. The SSM/I actually has seven channels providing measurements at 19H, 19V, 22V, 37H, 37V, 85H and 85V GHz, where the H, V refer to horizontally and vertically polarized radiation. From these measurements, it is possible to infer the total mass of liquid water in a vertical column, which we will refer to as the liquid water path (LWP). To obtain information on the distribution of supercooled liquid water contents with height and temperature Lunnon (1993) proposed the use of a two-dimensional microphysical model, the Cox model, (Cox, 1988). The basic method involves running the Cox model with various peak vertical velocities, until the LWP produced by the model agrees with that inferred from the SSM/I data. The liquid water contents can then be extracted from the model as a function of height and temperature.

The use of satellite microwave observations to derive a climatology of supercooled liquid water contents has

already been undertaken by Curry and Liu (1992) using 18 Ghz and 37 Ghz data from the Nimbus-7 Scanning Multichannel Microwave Radiometer. The LWP was derived using the method of Takeda and Liu (1987). The key difference from the method used here lies in the way the liquid water was distributed in the vertical to match the diagnosed LWP. Curry and Liu (1992) used the US Air Force Three-Dimensional Nephanalysis, which provides total cloud cover, cloud amount at 15 levels, heights of the lowest bases and highest tops and types of low, middle and high cloud. Given a cloud-base height from the Nephanalysis, the adiabatic liquid water content profile was calculated from cloud base temperature and pressure obtained from the European Centre for Medium-Range Weather Forecasts initialized analyses. The ratio of the actual liquid water content to the adiabatic value was assumed to decrease with height z as exp(a-bz). The coefficient b was set to 0.0012 m^{-1} to model the variation of the ratio with height reported by Skatskii (1965) and Warner (1970) for convective clouds. The coefficient a was adjusted at each SSM/I pixel so that the vertical integral of the LWC profile matched the diagnosed LWP. Curry and Liu (1992) mainly report results for supercooled single layer clouds. The advantage of this technique is that it uses available data on cloud structure, whereas we rely on the Cox model to produce the correct structure. The disadvantage is that it is not clear how well the variation of actual to adiabatic liquid water content with height in convective clouds reported by Skatskii (1965) and Warner (1970) applies to frontal clouds.

2.2 Derivation of LWP from SSM/I Data

A variety of methods have been developed to derive LWP from the SSM/I brightness temperatures. The current methods only work over the ocean because they rely on the low and essentially predictable emissivity of the sea surface. The low emissivity means that the ocean has a low brightness temperature at SSM/I frequencies. Emission by cloud and raindrops causes an increase in the observed brightness temperatures which can be related to the intervening LWP. Ice has a negligible emission relative to water, but scattering by ice and raindrops can decrease the observed brightness temperatures. The effect of scattering increases with increasing frequency. The observed brightness temperatures are also affected by surface wind speed, since the sea-surface emissivity increases with increasing wind speed, and by the atmospheric water vapour path. Thus, information on these is required and can be inferred from observed brightness temperatures or supplied independently.

A common approach is to use an algorithm which diagnoses LWP from a combination of brightness temperatures. The algorithms have been developed, either by relating observed LWPs to SSM/I brightness temperatures statistically or from a simplification of the full radiative transfer theory. The latter type of algorithm generally incudes a simplified description of the atmosphere, so that atmospheric temperature and humidity profiles are not input explicitly.

Seven algorithms were evaluated theoretically by Penney (1994). He applied a radiative transfer model developed by English (1991) to a global climatology of radiosonde ascents. Model clouds of known LWP were inserted into the soundings and the seven brightness temperatures calculated. These were fed into the algorithms to diagnose the LWP, which could then be compared with the true value. It was concluded that the algorithm due to Greenwald et al. (1994) (which will be referred to as the Greenwald algorithm) agreed best with the actual LWPs used in the radiative transfer calculations. An overall error of around 40 gm^{-2} was inferred. However, it is important to note that no account of the effects of rain was taken in the formulation of the Greenwald algorithm and neither did Penney (1993) consider these effects. Therefore, Penney's conclusions only apply strictly to the application of the Greenwald algorithm to layer clouds comprised entirely of cloud drops.

Despite the caveat above, the Greenwald algorithm was selected to derive LWP in this study, since when the project started we had no method of testing the algorithms when applied to rain. The algorithm requires sea-surface temperature as input and this was obtained from monthly mean global fields derived from 6-hourly analyses used by the Met. Office Unified Model. The Unified Model is the basic numerical prediction model used by the Met. Office and is run at different resolutions for different purposes, (Cullen, 1993). Analyses from the global version, with a resolution of 0.8° x 1.25° were used here. Surface windspeed was also taken from the

Unified Model analyses. The Greenwald algorithm assumes that the cloud emitting temperature is 6°C colder than the sea-surface temperature, so tropospheric temperature data were not required.

2.3 The Cox Model

The Cox model is a two-dimensional diagnostic microphysical model. The initial velocity, temperature and humidity fields have to be prescribed. These were obtained from archived analyses of the Unified Model for 00, 06, 12 and 18 UTC. The velocity fields are invariant during the course of an integration, because the model contains no dynamics, but the humidity and temperature fields evolve in response to condensation/evaporation and associated latent heat changes.

The Cox model is derived from that of Rutledge and Hobbs (1983). The model includes autoconversion of cloud water to rain water, initiation of the ice phase on a Fletcher ice nucleus spectrum, diffusional growth of rain and snow and accretion of cloud water by rain and snow. Graupel is also included, as in Rutledge and Hobbs (1984), but did not form during most of the integrations described here. The model contains a bulk water treatment of the microphysics. The form of the hydrometeor size distribution is specified, so that by integrating over the size distribution, diffusional growth, accretion etc. become functions of the species mixing ratios. In both models, the rain and snow size distributions are assumed to be exponential ie $N(D)=N_0\exp(-\lambda D)$. Rutledge and Hobbs (1983) assumed that N_0 is constant, while Cox (1988) made N_0 a function of temperature, to account for enhanced aggregation at warmer temperatures. Other differences are that Rutledge and Hobbs (1983) used separate cloud ice and snow classes but these are combined into one class in the Cox model. Cox also changed the specification of the snow terminal velocities for closer agreement with the empirical relationship between precipitation rate and ice water content found by Heymsfield (1977) and allowed the density of snow to vary with particle diameter. Rutledge and Hobbs used a constant snow density.

3. Initial Evaluation using CASP II Data

3.1 CASP II Overview

Data for validation were obtained from the Canadian Atlantic Storms Program, Phase II (CASP II), supplied by Atmospheric Environment Service (AES) , Canada. CASP II was undertaken by AES with the support of Boeing and Airbus. The CASP II data were obtained from a specially instrumented aircraft, based at St John's, Newfoundland and operating within a radius of 800 km. The aircraft was equipped with a comprehensive set of cloud physics instruments, as described by Cober et al. (1995). The key data for the initial evaluation were liquid water contents measured with a short-wire King Probe. Boeing provided us with a climatology of supercooled liquid water contents, similar to the FAR 25 climatology, derived from the CASP II data. It was planned to apply the SSM/I - Cox model technique to most of the CASP II cases and produce a climatology of supercooled liquid water content for comparison with that provided by Boeing. This was never done because of the problems encountered with the technique which are the subject of this report.

The CASP II flights were designed specifically to study the microphysical and dynamical properties of East Coast winter storms, in order to evaluate the potential for aircraft icing and also to help improve icing forecast models. A key feature for the purposes of evaluating our proposed technique was that CASP II flights were made coincident with SSM/I overpasses if possible and nearly always within a couple of hours of an overpass. The CASP II flights spanned the period 22 January 1992 to 15 March 1992. The edge of the sea ice moved south of Newfoundland during this period. Ice charts were obtained from the Met. Office Central Forecast Office (CFO) to ensure that only flights over the open sea were used, where the SSM/I can be used to diagnose LWP.

3.2 Synoptic Situation

The first CASP II case studied was 5 Feb. 1992, when a wave depression passed south of Newfoundland. Figure 1 shows the position of the fronts at 00 UTC as analysed operationally by CFO. It can be seen that the system was only partially occluded at this time. The track of the instrumented aircraft is shown by the dashed line on Fig. 1. The aircraft took off at from St John's at 2215 UTC, passed over the warm sector around 00 UTC and returned to St John's at 0215 UTC.

Unfortunately there are no synoptic observations from near the warm front and only one in the warm sector, at 18 UTC, near the cold front at 38.5°N. This reported a temperature of 16°C, light rain and 8/8 stratus at 200 ft. North of the low centre there were many observations of light to moderate continuous snow and screen temperatures over land were -5°C to -8°C.

3.3 SSM/I Data

Only data from the DMSP F11 satellite was available to us and this passed over Newfoundland two hours prior to the flight, at around 2035 UTC. Examination of the CFO charts for 18 UTC on 5th , 00 and 06 UTC on 6th, showed that the depression and associated fronts were moving with a fairly constant speed. This allowed a good estimate to be made of the frontal position at the time of the SSM/I overpass. The shaded area on Fig. 1 shows the position of the area containing SSM/I diagnosed LWPs in excess of 100 gm^{-2} in the vicinity of the fronts. This has been advected with the fronts from the estimated frontal position at 2035 UTC. The field of LWPs is not shown, since the details will probably have changed by 00 UTC. However, the general range of values is of interest, since this will determine the distribution of liquid water contents produced by the proposed technique. Figure 2 shows the LWP along 2 lines across the warm sector roughly normal to the fronts. The solid line in Fig. 2 is the southernmost sample. It can be seen that values up to 400 gm^{-2} are found and in the southernmost section these occur over 5 pixels, around 200 km. Examination of the SSM/I diagnosed LWP fields for other CASP II cases showed that values up to 400 gm^{-2} extending over several hundred kilometres were common.

3.4 Aircraft Data

The aircraft flew from St John's, Newfoundland to the warm sector at 5.5 km. The temperature was around -27°C at this altitude. Notes on the flight obtained from Boeing report small ice crystals only. We have no 2-D cloud probe data but the 2-D precipitation probe, which produces shadow images of hydrometeors in the size range 200 to 6400μm, gave concentrations of 2 - $6x10^4$ m^{-3}. These are rather higher concentrations than implied by the Cox model snow size distribution parametrization, which for the snow mixing ratios shown in Fig. 4 gives total concentrations of $4x10^3$ - $2.4x10^4$ m^{-3}. The aircraft made a continuous descent to 1 km in the warm sector and flew at this level through the cold front. The maximum temperature was 9°C and typically 2 - 6°C at 1000 m. Supercooled liquid water contents reached 0.09 gm^{-3} during the descent (Fig. 6) and the FSSP concentration was only around 20 cm^{-3}.

The aircraft flew north again behind the cold front and ascended in stages, with level runs in between. The supercooled LWC peaked at 1 gm^{-3} during a level run at 2000 m, causing rapid icing on the aircraft according to Boeing's notes. The LWC was generally around 0.2 gm^{-3} at this altitude. The FSSP concentration peaked at 400 cm^{-3} in the LWC peak. This may well be genuine, rather than being caused by scattering from ice crystals, because the 2-D probe count were around zero (although 2-D cloud probe data are required to be more certain). The large peak in LWC and high concentration are symptomatic of large ascent rates and so are in accord with synoptic observations of post-frontal convection caused by very cold air flowing south over the warmer sea.

During the final descent into St John's at 0215 UTC, two cloud layers were observed. The upper cloud layer was

all ice but supercooled LWCs of 0.2 to 0.5 gm^{-3} were measured in the lower cloud layer at -9 to -13°C. This illustrates how a vertical gap in the cloud can affect the occurrence of supercooled liquid water, if the lower cloud layer has insufficient ice nuclei to cause glaciation and it is not being seeded by ice crystals from the upper layer.

3.5 Cox Model Simulations

Analyses from the Unified Model were only available every 6 hours, so the 00 UTC analysis was used on this occasion. Allowance had to be made for the movement of the system, because when model profiles from the location at 2035 UTC of the SSM/I LWP feature were used to initialise the Cox model, no cloud formed. This was because by 00 UTC this region was behind the cold front and was too dry to produce frontal cloud.

The 00 UTC surface relative humidity and temperature analyses showed the presence of a moist, warm feature in approximately the same location as the warm sector on the 00 UTC CFO chart. Therefore, temperature, relative humidity and wind profiles were extracted from the vicinity of this analysed feature. The temperature at 5.5 km from the model analysis was -27°C in excellent agreement with the aircraft value. Within the vicinity of the warm sector the model analysis had a surface temperature of 2 - 11°C and the temperature at 1 km was 0 - 4°C. The latter temperatures are 2°C colder than generally observed.

The profiles from the UM analyses were used without modification where possible. Temperature, relative humidity, u and v components of wind were available at 9 levels from the surface to 200 mb. Relative humidity was available at 6 levels from 950 mb to 300 mb. However, vertical velocity (w) was only available at 4 levels (850, 700, 500, 250 mb) and, as described later, this was not always sufficient to capture important features of the profile. The temperature and relative humidity profiles were interpolated onto the Cox Model grid. The same profile was applied at all locations in the horizontal. The crude w profile had to be smoothed as well as interpolated, to avoid unrealistic spikes developing in the LWC profile. Although some Cox model runs used the (smoothed) w values from the analyses, in most runs the they were multiplied by a factor of 2 - 5 to increase the LWP for closer agreement with the SSM/I value. Since the Cox model is two-dimensional, the u, v wind components were combined into one velocity $(u^2 + v^2)^{0.5}$, which was assumed to be in the plane of the Cox model and directed from left to right. A problem left unresolved was how well a two-dimensional model can represent a three-dimensional system. An indication that there may sometimes be a problem is given in Section 5. The horizontal velocities were progressively adjusted from the left-hand boundary to satisfy the continuity equation. These were adjusted, rather than the vertical velocities, because we wished to retain precise control of the latter. This adjustment occasionally resulted in inflow from the right-hand boundary.

The Cox model was run with a horizontal grid spacing of 1 km, a vertical grid spacing of 200 m and a timestep of 8 seconds. Prior experimentation showed that increasing the timestep from 1 to 8 seconds made only a minor difference to the solution. The values at the left and right hand boundaries were held constant during the integration (rather than using cyclic boundary conditions), implying that air flowed through the model . The model was run to equilibrium. The time taken to achieve this varied with w and to ensure equilibrium the model was normally run to 12000 seconds.

Initial attempts at running the Cox model for 5 Feb. 92 case were beset by many difficulties which are not detailed here. The first of the final attempts to simulate SSM/I diagnosed LWP values used input profiles from 44.5°N, 56.2°W, ie on the occlusion north of the warm sector. The smoothed w profile peaked at 0.09 ms^{-1} and this produced zero LWP due to cloud in the presence of precipitation and this was also true when the w values were doubled. The contribution of rain to the LWP was also negligible because the freezing level was near the surface. Profiles were then sought exhibiting the highest temperatures and relative humidities together with substantial regions of ascent, since the preliminary simulations indicated that such profiles would produce the largest cloud LWP values. Profiles were used from around 43°N, 54°W, 41.8°N, 53°W and 41.5°N, 54°W. Two of these locations were behind the cold front according to CFO charts, but the 1.5 m temperature field from the

Unified Model analysis suggested that they were in the warm sector. Although profiles from farther east exhibited a high relative humidity, they had progressively lower temperatures and the vertical velocity peaked at higher altitudes. Both these factors lead to lower LWP. Therefore, the analysis concentrated on the use of the profiles detailed above, since it was proving difficult to make the Cox model produce the largest LWP values diagnosed from the SSM/I data.

Figure 3 shows the profiles used to initialise the Cox model from 41.5°N, 54°W (the w profiles are unsmoothed). Figure 4 shows equilibrium cross sections of cloud liquid water and snow mixing ratios in g Kg^{-1} resulting from the use of the profiles in Fig. 3, but with the vertical velocities doubled. The horizontal velocity profile also had 15 ms^{-1} subtracted from the values shown in Fig. 3 in order to constrain the equilibrium solution to lie within the model domain. Preliminary numerical experiments showed that this did not alter the equilibrium LWP values. The surface rainfall rate is also shown in Fig. 4c. It can be seen from Fig. 4a that as air from the right-hand boundary ascends, cloud forms as liquid water, much of it supercooled. Peak values are around 0.3 gKg^{-1} between 40 and 70 km. The initial column of cloud liquid water is tilted because the horizontal velocity increases with height. In model runs without windshear the initial column is upright. Ice and snow (all in the snow category) start to develop around 30 - 40 km downstream and as the snow grows it depletes the supercooled cloud liquid water. About 2/3 of the depletion is due to diffusional growth of the snow and 1/3 due to accretion of supercooled water by the snow. Therefore, the initial peak in LWP occurs where cloud has recently formed in air ascending from the left-hand boundary and there has not been time for snow to develop. When cloud first forms in the model there are large LWP values and large supercooled liquid water contents throughout the horizontal domain, because snow has not had time to develop.

The behaviour of the cloud liquid water field in Fig. 4a is very similar to results presented by Zawadzki et al. (1993), who developed a microphysical model similar to the Cox model, again based upon the Rutledge and Hobbs model. They simulated a frontal case from the first phase of the CASP project, using w and u fields obtained from observations and so which varied in the horizontal. Thirty minutes from the start of the integration there was supercooled cloud water throughout the 200 km model domain. However by 120 minutes, supercooled water had disappeared, apart from near the upwind cloud edge. They stated that this is in accord with the observations. They also suggested that observed regions of supercooled liquid water in frontal systems are mainly associated with embedded convection.

Figure 5 shows equilibrium LWP as a function of distance from four integrations of the Cox model. These are based on the profiles in Fig. 3 but with 15 ms^{-1} subtracted from the horizontal wind speeds and the vertical velocities multiplied by a factor 1, 2, 4, 8 in Figures 4a to 4d respectively. This produced maximum vertical velocities of 0.066, 0.132, 0.264 and 0.528 ms^{-1}. The thin dashed line shows the total LWP, the dotted line the contribution to LWP from supercooled cloud water and the solid line the contribution from cloud water above 0°C. The total LWP including the contribution from rain is shown by the thick dashed line. Rain only exists at temperatures above 0°C in all these integrations. These plots are typical of runs of the Cox model with the w profile invariant in the horizontal. They comprise an initial peak, around 80 km width, which tails off to a region where LWP varies little with distance. This is where the cloud and precipitation have come into equilibrium and so will be referred to as the equilibrium region. The initial peak occurs where precipitation has not had time to form. Increasing the vertical velocity increases the cloud LWP in the equilibrium region by a lower factor than in the initial peak, at least in Figures 5a to 5c. This suggests that the enhanced generation of cloud water by a larger vertical velocity is partially offset by enhanced removal by precipitation, since more precipitation is also generated. Such behaviour increases the difficulty of matching the diagnosed LWP values in the equilibrium region.

The equilibrium region in Figures 5a, 5b contains virtually no supercooled cloud water. An equilibrium LWP of around 100 gm^{-2} due to supercooled cloud water is apparent in Fig. 5c and 180 gm^{-2} in 5d. Thus, increasing the vertically velocity eventually overcomes glaciation, even though the snow mixing ratios are also increased. Rain also makes an increasing contribution to the LWP as the vertical velocity is increased. This is masked

somewhat in Fig. 5c and especially in Fig. 5d by the lowering of the freezing level in the region from 70 to 120 km, due to the melting of the larger snow flux. This reduces the depth of atmosphere containing rain. The inclusion of rain produces an LWP value of 300 gm^{-2}, in Fig. 5b and 400 - 500 gm^{-2} in Fig. 5c. These values are similar to those diagnosed from the SSM/I data. However, in Fig. 5c they are accompanied by virtually no supercooled cloud water, while supercooled liquid water was evident in the aircraft data.

The profile of cloud liquid water content measured by the aircraft during the descent in the warm sector is compared in Figures 6 and 7 with equilibrium profiles from the Cox model at 60 km, 120 km and 160 km from the left hand boundary. Liquid water content is plotted against height in Fig. 6 and against temperature in Fig 7. The Cox model was run with profiles from 43°N, 54°W, since these gave the largest LWP for a given peak ascent rate and also because they were close to the aircraft descent in the warm sector. The LWP values appeared to be maximised by these initial conditions because the vertical velocity peaked low down and only declined slightly at higher levels. No attempt has been made to match the LWP due to cloud from the Cox model with that implied by the observed LWC profile shown in Fig. 6a. The model-predicted LWP was 150 gm^{-2}, with 90 gm^{-2} from above 1 km (all supercooled), where the aircraft descent terminated. The observed LWP was 55 gm^{-2}, with around 45 gm^{-2} supercooled. This means the LWC values in the model are larger than those observed. The model profile at 60 km (Figs. 6b, 7b) differs from the observed one in that it peaks higher in the atmosphere, at 3 km instead of 2 km and around -11°C instead of 0 to -3°C. This region is in the downstream wing of the initial LWP peak, where snow has only partially depleted the supercooled cloud water. The model profile at 120 km (Figs. 6c, 7c) is in reasonable agreement with the observed one, although the model LWCs are about twice as large. The major region of supercooled liquid water is at temperatures warmer than about -5°C, both observed and modelled. The agreement between the observed and model liquid water feature around 5 km, or -20°C to -30°C is probably spurious, given the likely horizontal variability of supercooled LWC. This feature disappears from the model by 160 km due to glaciation, Figs. 6d, 7d. Otherwise the model profile is similar to that at 120 km.

The model run shown in Figs. 6 and 7 was repeated using the raw (smoothed) w values from the Unified Model analysis (ie reduced by a factor of 2), to see if the observed and modelled LWCs could brought into better agreement. However, the low-level maximum in LWC of 0.2 gm^{-3} in Figs. 6d and 7d remained but the supercooled water disappeared above -3°C. After the descent, the aircraft flew at 1 km for around 30 minutes and measured LWC values of up to 0.3 gm^{-3}, about 10 minutes after the descent, which is more in accord with the model results shown in Figs. 6 and 7.

In summary, we wished to make the Cox model match SSM/I diagnosed values of 200 - 400 gm^{-2}. This proved difficult unless the Cox model was initialised with the broadest vertical velocity profile and warmest temperature profile from the Unified Model analysis. Using profiles from 41.5°N, 54°W and a peak vertical velocity of 0.13 ms^{-1}, total LWP values of 300 gm^{-2} were produced in the equilibrium region accompanied by rainfall rates of 1.5 - 2 mmh^{-1}. Values of up to 500 gm^{-2} were achieved with a peak vertical velocity of 0.26 ms^{-1}, accompanied by rainfall rates of 3 - 4 mmh^{-1}. Cloud water contributed 100 gm^{-2} and 150 - 200 gm^{-2} respectively to these totals and supercooled cloud only made a contribution (90 gm^{-2}) with the higher vertical velocity. Rain water contributed 200 gm^{-2} and 300 gm^{-2} respectively.

The low contribution from cloud water is in accord with the LWC measurements from the aircraft in the warm sector. Boeing have provided a table of LWP values derived from all the aircraft profiles obtained during CASP II. Many of the profiles were through a restricted height range and terminated in mid troposphere. Table 1 shows a histogram of the LWP values (i) from profiles sampling down to at least 4000 ft and (ii) obtained during take off and landing. The latter have been separated out because they go down to the surface and also because they might not be representative of the observational area. Table 1 shows that in-situ cloud LWP values greater than 200 gm^{-2} were quite rare and a value of 55 gm^{-2}, as measured in the warm sector on 5 Feb. is fairly typical of the CASP II data.

Table 1. Histogram of cloud LWP values derived from CASP II aircraft profiles

LWP (gm^{-2}) Class	> 0 - 50	50 - 100	100 - 200	> 200
(i) Profile down to at least 4000 ft	10	4	3	1
(ii) Profile on take off, landing	6	4	2	1

In order to close the gap between LWP values derived from measured cloud LWC profiles and typical SSM/I values in frontal cases of 300 - 500 gm^{-2}, a contribution from rain and/or from cloud beneath the base of the profile must be assumed. The possibility that the SSM/I diagnosed value is an overestimate is considered in Section 6. The Cox model provides the extra LWP from the rain contribution but for 5 Feb. 92 case this requires widespread rainfall rates of 1.5 - 4 mmh^{-1}, which may be on the large side for a warm sector. The Cox model does not have a boundary layer scheme and can only generate cloud by steady ascent, not from mixing. There is potential for low-level cloud to make a significant contribution to the LWP. For example, for a 500 m deep cloud with a base temperature of 2.5°C, the adiabatic LWP is around 200 gm^{-2} and this varies as the square of cloud depth, so a 700 m deep cloud would have an adiabatic LWP of around 400 gm^{-2}. Given the one observation of cloud base at 400 ft in the warm sector on 5 Feb. 92, there is sufficient unsampled depth of atmosphere beneath the aircraft to yield a significant contribution to the LWP. On the other hand, Table 1 shows that profile measurements on take off and landing do not produce significantly larger LWPS than profiles terminating higher up.

Although the Cox model was finally made to achieve the diagnosed LWP values, there were doubts over the solution because of the large rain contribution required. Also, although the occurrence of a maximum of supercooled cloud water content (and hence maximum LWP) near cloud-edge is in accord with the results of Zawadzki et al. (1993), the maximum occurred where there is no precipitation. This is in contradiction to the view which is widespread in the literature that precipitation is associated with the larger LWP values. Takeda and Liu (1987) deduced that an LWP of 200 gm^{-2} was required for 50% of cold deep clouds to be precipitating and 600 gm^{-2} for warm shallow clouds. All clouds with LWP in excess of 1000 gm^{-2} were precipitating. A cloud was classified as precipitating if the LWP estimate from 18 GHz exceeded that from 37 GHz by more than 100 gm^{-2}, a limit determined by comparison with surface observations. It should be noted that they used data from 20 - 30°N, so the freezing level should be much higher than in the cases simulated here, thus increasing the LWP due to rain for a given rain rate. Following Takeda and Liu (1987), Curry and Liu (1992) assumed that precipitation is associated with LWP values greater than 500 gm^{-2}, a criterion also used by Greenwald et al. (1992). Grody and Ferraro (1992) assumed an LWP value of 300 gm^{-2} for precipitation, but no source was given. Lin and Rossow (1994) classified clouds as precipitating if T37V - T37H < 37°C. Using the Greenwald algorithm they found that 50% of cold clouds were classified as precipitating at an LWP of 400 gm^{-2} and all cold clouds were so classified at 600 gm^{-2}. However, they noted that all the criteria referenced here had not been well-validated.

4. Investigations in the vicinity of the UK

A limitation of the CASP II data is that we do not have any conventional satellite or radar data, so can only relate the SSM/I LWP field to synoptic charts. No information is available on whether large LWP values coincide with precipitation or warm cloud tops (although in the region of the aircraft track on 5 Feb. 92 the cloud top was above 5.5 km). Therefore, a limited, mainly subjective, investigation was undertaken in the vicinity of the UK, using satellite and radar data. The data came from January 1993, during which many frontal systems crossed the UK. The SSM/I derived LWP fields on seven days were compared visually with infrared and visible Meteosat images and with the composite image from the UK weather radar network. Only the SSM/I LWP fields in the vicinity of frontal system were studied, not the more straightforward case of anticyclonic

stratocumulus. Of course, there can also be stratus or stratocumulus in the vicinity of frontal systems.

Only the conclusions of the study are presented here.

(i) Diagnosed areas of LWP greater than 200 - 500 gm^{-2} were consistently found in association with fronts and their dimensions were around 300 - 600 km by 150 km. There were often areas with LWP diagnosed to in excess of 600 gm^{-2} of this size.

(ii) When a front was sampled on two SSM/I overpasses, generally 10 - 12 hours apart, the mesoscale areas of large LWP were seen to persist, although the detailed pattern of the field changed. (This suggests that the problem with our simulation of 5 Feb. 92 was not the time difference between the SSM/I overpass at 2035 UTC and the 00 UTC Unified Model analysis used to be initialise the Cox model.)

(iii) There was some evidence that large LWP values were associated with precipitation but this was not always so. There was little correlation between the shape of the areas of heavy precipitation and the shape of the high LWP features. The comparison with radar data could only be made over the sea and so was often at moderate to long range from the radars, which introduced some uncertainty.

(iv) Large LWP values were not obviously related to the cloud-top temperature field. They occurred where there was both a warm and cold cloud top. In warm front cases there was a tendency for the areas of large LWP to straddle a region of large infrared temperature gradient where the warm conveyor belt could be expected to be ascending the warm frontal surface. These areas may be associated with significant rainfall rates but they were beyond radar range in the cases examined, so this could not be confirmed.

(v) The pattern of LWP values was such that the maximum values were found towards the centre of the field and then decreased roughly equally towards all edges. There was not a peak close to one edge, as produced by the Cox model and by Zawadzki et al. (1993).

This study indicated the ubiquitous nature of mesoscale areas of SSM/I diagnosed LWP values of several hundred gm^{-2}, in association with frontal systems. The values tended to be larger than those from the CASP II cases, possibly because the low-level temperatures were higher. Published LWP values for the North Atlantic frontal systems are limited because most SSM/I studies have concentrated on lower latitudes and have often produced average values which may or may not include zeroes. Prigent et al. (1994) diagnosed mesoscale areas with LWP > 500 gm^{-2} along a cold front. Liu and Curry (1995) show LWP fields for 10 and 31 January 1993 which have mesoscale areas in excess of 500 gm^{-2}. We also looked at 10 January 1993 near the UK and produced similar results to Liu and Curry (1995). Lin and Rossow (1994) showed a histogram of LWP values for clouds from 20 - 50°N with tops colder than 0°C. For non-precipitating clouds the mean LWP was 47 gm^{-2} but for precipitating clouds it was 683 gm^{-2}, indicating that large LWP values were widespread.

The UK SSM/I data (and 5 Feb. 92 CASP II data) were used for two minor investigations of the possible affect of raindrops and ice crystals on the Greenwald algorithm. A few LWP fields were rederived from the SSM/I data using the algorithms of Liu and Curry (1993) and Karstens et al. (1994). These algorithms were developed to work in the presence of rain. The resultant LWP values were not significantly different from the Greenwald values. It should be noted however that a theoretical study of the Greenwald algorithm described in Section 6 found that rain may cause the Greenwald algorithm to overestimate the true LWP of rain by up to 60% (at a true value of 500 gm^{-2}).

A small study was undertaken to see if scattering from ice crystals and rain drops could be affecting the Greenwald LWP estimates. Grody and Ferraro (1992) have developed a scattering index (SI) to detect precipitation from the effect of scattering on the 37 GHz or 85 GHz brightness temperatures. The scattering index is the difference between the observed brightness temperature and an estimate from the lower frequency

channels, which are assumed not to be affected by scattering. The estimate is obtained from a regression relationship between the lower and higher frequency channels obtained from data which excludes precipitation cases. For vertically polarized 37 GHz data, SI is given by :-

$$SI(37V) = Ti - Tb(37V)$$

$$Ti = 60.1 + 0.781\ Tb(19V)$$

where Tb is the observed brightness and Ti the estimate for non-scattering conditions.

A value of 7°C is used to unambiguously identify scattering due to precipitation. When applied to some of the UK SSM/I data and 5 Feb 92 case, this threshold was never exceeded. The 85 GHZ scattering index was also derived, since this is more sensitive, but virtually no values above the threshold were found. The 37 GHZ SI seemed more relevant however, since the Greenwald algorithm uses this frequency and not 85 GHZ. Thus, it is concluded that the SSM/I cases examined were not affected by significant scattering. It must be admitted that since scattering reduces the brightness temperatures, it seems likely to reduce the estimated LWP values, while we are looking for an overestimate.

5. Mesoscale Model Case Study

5.1 Background

Following a meeting at the Joint Centre for Mesoscale Meteorology (JCMM), University of Reading, to discuss the problems with the technique presented in Section 3, two further significant studies were performed. The Cox model and SSM/I derived LWPs were compared with those from an experimental version of the mesoscale version of the Unified Model. The accuracy of the Greenwald algorithm in the presence of rain was investigated using radiative transfer code obtained from the Remote Sensing and Instruments Branch, which had been developed by Kummerow et al. (1989). The Kummerow radiative transfer scheme allows for emission and scattering by rain and ice, unlike the radiation scheme used by Penney (1994) to test the Greenwald algorithm.

The operational version of the Unified Model contains a simplified description of the occurrence of supercooled water and ice. Cloud is assumed to be all water at 0°C and all ice at -15°C. The proportion of water to ice decreases according to a prescribed function between these limits. A new scheme has been developed to calculate explicitly the mixing ratios of water and ice (Ballard and Hutchison, 1995). The new scheme, as applied to the case study, is essentially that of Rutledge and Hobbs (1983), but uses a combined prognostic ice/snow variable, as does the Cox model. (The new scheme has been modified subsequently. For example, fall speed of ice/snow has been increased compared to that used in Rutledge and Hobbs (1983) and in the Cox model)

A detailed comparison of a version of the mesoscale model containing the new microphysical scheme, the Cox model and SSM/I derived LWPs was undertaken for 9 Nov. 1993. This day was chosen because it had already been subject to detailed study at the JCMM. An SSM/I overpass occurred at 1945 UTC, which covered the North Sea. The comparison used an available 36 hour forecast from the experimental version of the mesoscale model, verifying at 18 UTC.

During 9 Nov. 1993, an occlusion advanced steadily southeastwards across the UK, to lay from SW Wales to NE England by 18 UTC, Fig. 8. By this time the occlusion had become stationary over the southern UK. It continued to move eastward farther north and lay about 150 km east of Scotland by 18 UTC. Examination of the infrared Meteosat imagery and the UK composite radar imagery suggested that the occlusion tended to have the structure associated with a split cold front (Browning and Monk, 1992). A split front is associated with dry mid-tropospheric air overrunning the surface front from the rear, producing an upper front in advance of the

surface front. Between the two fronts there can be light precipitation associated the shallow cloud layer, or convection can break out if the overrunning dry air produces potential instability. The cloud top height increases abruptly at the upper front and a band of heavier rain is generally aligned along the upper front. The 9 Nov. is not a classic case. The cloud tops up to 100 - 250 km from the surface front were relatively warm, 0 to -20°C with only a moderately sharp transition to tops of -30 to -50°C farther east. The radar imagery showed a solid band of precipitation under the colder cloud, with more fragmented rain areas between the cold cloud and surface front.

The LWP field diagnosed from the Greenwald algorithm is shown in Figure 9. A band of LWP values in excess of 100 gm^{-2} stretched from the surface front to within 100 - 200 km of the eastern edge of the cold cloud. The band was composed mainly of values 200 - 300 gm^{-2} but there were two bands of larger values (300 - 500 gm^{-2}) running parallel to the main band. The most pronounced band lay between the surface front and the edge of the colder cloud. The eastern band was situated under the cold cloud and was more fragmented. The LWP values on this occasion were rather lower than found in the cases studied from January 1993.

5.2 Mesoscale Model Results

The 36 hour forecast from the mesoscale model was fairly accurate and captured the main features of the occlusion well. However, comparison of the model and observed precipitation and cloud fields indicated that the model had not advanced the front sufficiently to the east of Scotland. Figure 10a shows the mesoscale model LWP field (excluding the contribution from rain) at 18 UTC. When allowance is made for the positional error in the front and the 75 minute time difference from the SSM/I overpass, it can be seen that model LWP field pattern is in reasonable agreement with the SSM/I derived pattern. The model has captured the band of large LWP values on the western edge of the field, east of Scotland. It has also produced an indication of the band diagnosed further east, but only in the southern North Sea. The model LWP values also appear to be in much better agreement quantitatively with the values produced by the Greenwald algorithm than those from the Cox model. The model values in the western band of enhanced values are around 500 - 700 gm^{-2} compared to the SSM/I values of 300 - 500 gm^{-2}. The model values outside the western band are mainly around 100 - 200 gm^{-2} compared to the majority of the area being diagnosed as 200 - 300 gm^{-2} or larger in the eastern band of enhanced values. The model LWPs exclude the contribution from rain, which has not been computed as a field, because rainfall rate profiles are not available from the archived model data. The contribution can be estimated approximately by assuming the surface rainfall rate remains constant to the freezing level and by assuming a Marshall Palmer drop-size distribution. The estimated contribution is around 100 gm^{-2} over most of the area decreasing to around 50 gm^{-2} over most of the band of enhanced LWP values in the west. Thus, adding in the rain contribution improves agreement with the SSM/I estimates over most of the field but slightly increases the model overestimate in the western band.

The good agreement between the mesoscale model and SSM/I LWP estimates is in marked contrast to the previous Cox model SSM/I comparisons. To help understand how the mesoscale model manages to generate larger LWP values than the Cox model, the contribution from cloud water colder than 0°C and warmer than 0°C has been computed separately and is shown in Figures 10b, 10c. It can be seen that where there are large LWP values, the major contribution comes from cloud warmer than 0°C. Supercooled cloud rarely contributes more than 200 gm^{-2} and over the majority of the field it contributes less than 100 gm^{-2}. Figure 10d shows the total mass of ice/snow in the vertical in gm^{-2} (IWP). The pattern is in accord with the split front concept, with large IWP values being associated with the colder cloud tops. The largest supercooled cloud LWPs occur where there is a low IWP, in agreement with the behaviour of the Cox model.

The mesoscale model produced a band of precipitation (not illustrated) whose boundaries nearly coincided with the boundaries of the cloud LWP field in Fig 10a. However, there appeared to be little correlation between the details of the surface rainfall rate and cloud LWP fields. The band of large LWP values east of Scotland was mainly associated with low rainfall rates, < 0.5 mmh^{-1}, although it extended into a region with rates of up to 1

mmh^{-1} in the north. Over England, even larger cloud LWPS were associated with maxima in rainfall rate eg NW England, SW England. On the other hand, equally large rainfall rates over the North Sea were associated with low LWP values. The supercooled LWP field was even less well correlated with the surface rainfall rate field. Had the model LWP field in Fig 10a contained the contribution from rain, there would have been some improvement in the correlation, but given the typical maximum rainfall rate of 1.5 - 2 mmh^{-1} and freezing level of 1500 m, it is doubtful that the rain contribution would be large enough to produce a high degree of correlation.

5.3 Cox Model Results

The Cox model was run for 6 locations detailed in Table 2. The locations were chosen using the 18 UTC surface chart and infrared satellite picture. Points 1 and 2 were where the mesoscale model and the observations indicated a lower cloud top and higher LWP. Points 3 and 4 were where there was a colder cloud top and lower LWP. The mesoscale model produced a region of large LWP values in SW England and the western English Channel, even though there was a cold cloud top, both observed and in the mesoscale model. Points 5 and 6 were selected to help explore the reason.

Table 2 Locations Selected for Cox Model Runs

Point Number	Latitude	Longitude	Comments
1	57°N	2.0°E	Midway between surface front and T=-20°C cloud top
2	55°N	2.0°E	Just on warm side of T = -20°C cloud top
3	54°N	2.9°E	Under cold cloud top
4	53°N	1.0°E	Just under T = -20°C cloud top
5	51°N	2.2°W	SW England
6	49°N	3.5°W	Near Channel Islands

The Cox model was initialised using UM archived fields for 18 UTC, as described in Section 3.4. The results of the model runs are summarised in Table 3, which shows the factor by which the archived vertical velocities were multiplied, the maximum vertical velocity, the LWPs due to cloud in the initial peak and in the equilibrium region and the LWP due to supercooled water in the equilibrium region. The maximum cloud-top height and associated temperature are also shown. The model top boundary was at 8 km in these runs and this sometimes limited the depth of cloud which formed. Experience suggests that had a deeper cloud been allowed to form, glaciation would have been enhanced, reducing the LWP values.

Run 1 produced a deep cloud and low LWP, with negligible supercooled water in the equilibrium region. This does not agree with the mesoscale model results and SSM/I observations which indicated a moderately low cloud top and large LWP in this region. Run 2 used the unadjusted archived vertical velocity (ie not multiplied by 2). Although this produced a lower peak LWP, the LWP in the equilibrium region was 4 times larger and half was due to supercooled water. The reason for this apparently paradoxical behaviour is that a lower, warmer cloud top was produced in run 2, so less ice was initiated. In general, increasing the vertical velocity eventually produces larger LWP and supercooled LWC values. However, run 2 shows that in cases where the relative humidity aloft is marginal for cloud formation, increasing the vertical velocity can produce a deeper, more

glaciated cloud.

Table 3. Summary of Results of Cox Model Simulations of 9 Nov. 93 Case

Run No.	Point No.	w Factor	w Peak (ms^{-1})	LWP Peak (gm^{-2})	LWP Eq. (gm^{-2})	Supercooled LWP (gm^{-2})	Cloud-top Height (km)	Cloud-top Temp. (°C)
1	1	x2	0.059	300	30	0	8.0	-40
2	1	x1	0.030	130	120	110	3.8	-13
3	2	x2	0.073	280	20	0	8.0	-38
4	3	x2	0.046	110	0	0	8.0	-37
5	4	x2	0.082	400	30	0	8.0	-37
6	5	x2	0.062	1080	200	100	5.0	-18
7	6	x2	0.054	1080	250	110	4.5	-12
8	1	x5	0.149	750	40	0	8.0	-42

Runs 3 and 4 produced a deep glaciated cloud, which is to expected since they apply to the region farther ahead of the surface front where both mesoscale model and observations indicated a higher cloud top and lower LWP. However, the LWP in the equilibrium region is much lower than produced by the mesoscale model and inferred from the Greenwald algorithm.

The relative humidity profiles from the UM archive for runs 6 and 7 (locations 5 and 6) contained a dry region in mid-troposphere and became moister higher up. This suggests that in reality and in the mesoscale model forecast there were two cloud layers, the lower one with a sufficiently warm top to inhibit glaciation. The Cox model runs only produced the lower cloud, the model top boundary probably being too low to allow the development of the upper cloud layer. The LWP produced by the Cox model was larger than in runs 1 - 5, but much less than from the mesoscale model, Fig. 10. These were the only integrations which produced supercooled liquid water, apart from run 2.

In order to explore reasons for the ability of the mesoscale model to produce LWP values which are more in accord with the observations than those from the Cox model, the mesoscale model fields have been examined in more detail by producing cross sections through the front at various locations. Figure 11 shows cross sections of ice/snow mixing ratio ($kgKg^{-1}$) and cloud liquid water mixing ratio ($KgKg^{-1}$), running E-W through Scotland into the North Sea at approximately 56.5°N. The height of the freezing level is also shown as a dashed line on Fig. 11b. The Scottish land mass stretches from around 100 - 400 Km on these cross sections.

The band of high LWP values east of Scotland can be seen as a low-level high liquid water content feature stretching from around 450 - 600 Km on Fig. 11b. There is little ice associated with this cloud feature, except for a finger above 800 mb extending from the ice cloud farther east, Fig. 11a. The cloud top temperature is around -5°C. The low-level cloud feature appears associated with a low-level vertical velocity maximum of around 0.065 ms^{-1} at 900 mb (around 1 km). There is little ascent above 700 mb. The low-level liquid water cloud nearly disappears between 600 and 670 km, which is a region of low level descent. Between 700 and 870 km there is ascent throughout the troposphere but with two maxima at around 500 and 900 mb. This has generated a deep, virtually glaciated cloud, but with a low-level liquid water feature, mainly beneath the freezing

level. In general, it could be misleading to relate cloud features to vertical velocity features on a cross section perpendicular to a front, because the flow will be mainly along the front and the cloud pattern could be related to vertical velocity features downwind of the cross section. However on this occasion, the same cloud features are seen on cross sections further south, suggesting a degree of along-front coherence of the vertical velocity field.

Several further runs of the Cox model were performed, altering the initial conditions for Point 1 in an attempt to reproduce the low-level liquid water cloud east of Scotland developed by the mesoscale model. The key differences between the mesoscale model forecast and Cox model in this region appeared to be :-

(i) the vertical velocity profile peaked at 1 km in the mesoscale model, but around 5 km in the smoothed profile derived from the Unified Model analysis

(ii) the mesoscale model cloud top was around 2.5 km, with a temperature around -5°C

(iii) the mesoscale model temperatures were a few degrees higher, producing a higher freezing level and hence a greater LWP due to water above 0°C.

Table 4. Summary of Results from Further Simulations of Point 1

Run No.	Initial Conditions	LWP Peak (gm^2)	LWP Eq. (gm^{-2})	LWP Super-cooled (gm^{-2})	LWP Total, inc. Rain (gm^{-2})
9	As run 1, but T, w from mesoscale model	450	100	10	190
10	As run 10, but RH increased to 100% down to surface	610	120	10	210
11	As run 10, but RH reduced to 50% above 3 km	510	200	90	260
12	As run 10, but T increased by 2°C and RH reduced to 50% above 2.6 km	750	370	140	450

The additional runs are summarised in Table 4. In run 9 the vertical velocity and temperature fields from the Unified Model analysis were replaced with profiles derived from the mesoscale model at around 500 km, Fig. 11. Compared to run 1, the equilibrium LWP increased from 30 to 100 gm^{-2}, but because a deep, glaciated cloud was produced, the LWP through supercooled cloud was only 10 gm^{-2}. Run 10 used the same initial conditions as run 9 except that the relative humidity was increased to 100% from 4 km to the surface. This had most impact on the initial LWP peak but the downstream equilibrium LWP was only increased to 120 gm^{-2} and the supercooled component was unchanged. The relative humidity above 3 km was reduced to 50% in Run 11 to produce a cloud of similar depth to that in the mesoscale model. This limited the cloud-top height to 3.6 - 3.8 km and temperature to -8 to -11°C. This produced an equilibrium LWP of 200 gm^{-2}, with a supercooled cloud contribution of 90 gm^{-2}. The cloud produced by the Cox model was still deeper than in the mesoscale model and the freezing level was lower. Therefore, in run 12 the initial temperatures were increased by 2°C and the relative humidity reduced to 50% above 2.6 km. This produced a cloud top around 3.3 - 3.4 km with a temperature of -5 to -8°C, similar to the mesoscale model. The equilibrium LWP was increased to 370 gm^{-2}, with a supercooled cloud contribution of 140 gm^{-2}. Table 4 also shows the total LWP in the equilibrium region, including the contribution from rain, which was around 60 - 90 gm^{-2}.

The total is 450 gm^{-2} which is in good agreement with the maximum the Greenwald SSM/I estimates of 400 - 500 gm^{-2} but a little below the mesoscale model values of around 500 -700 gm^{-2}.

These simulations highlight the sensitivity of the degree of glaciation to the cloud-top temperature. The Cox model developed a much deeper cloud at Point 1 than the mesoscale model, or implied by the observations (unless the vertical velocity was very small as in run 2). There are two likely reasons. Either the 18 UTC Unified Model analysis was too humid aloft, or in the mesoscale model (and in reality) drier air was overrunning the surface front, as in the split-front model of Browning and Monk (1982). The Cox model would require initialisation with a spatially varying humidity to simulate the latter and a realistic simulation would probably require a 3-D model. When the Cox model is forced to produce a cloud of comparable depth to that in the mesoscale model at Point 1, there is less glaciation and a more realistic LWP. However, there is more glaciation than in the mesoscale model, possibly because even in run 12 the Cox model cloud-top temperature was still lower than in the mesoscale model.

The Cox model has also been rerun for point 3, where there is a deep cloud, using vertical velocity and temperature profiles from the mesoscale model at around 800 km. The main difference from the original run is a low-level w peak at 1km. The equilibrium cloud LWP is increased from 10 to 50 gm^{-2}, which is less than half that in the mesoscale model forecast and much less than the Greenwald estimates which are mainly in excess of 200 gm^{-2}. Even adding in the rain contribution of around 60 gm^{-2} to give a total of 110 gm^{-2}, the typical Greenwald estimate is not achieved, although it is approached more closely. Neither the Cox model nor the mesoscale model produce LWP values which approach the largest SSM/I values of around 500 gm^{-2} in the eastern band of large values.

Finally, the Cox model was rerun for point 3, using the archived Unified Model profiles but with the vertical velocity multiplied by 20, to give a peak w of 0.73 ms^{-1}. This increased the initial peak LWP to greater than 1500 gm^{-2}, but the equilibrium value was only increased to around 100 gm^{-2}, most of which was due to supercooled cloud. The solution was still evolving at 12000 s, as the warm cloud was washed out, the rainfall rates varying from 2 to 8 mmh^{-1}. The rainwater contribution to the LWP was up to 300 gm^{-2} at the highest rainfall rate, making the total LWP comparable with the Greenwald estimate. However, it seems implausible that such high rates would have extended over the area covered by Greenwald estimates in excess of 300 gm^{-2} under the cold cloud. Also, as shown in the next section, such large rainfall rates do not appear compatible with the measured SSM/I brightness temperatures.

6. Investigations with the Kummerow Radiative Transfer Scheme

6.1 Accuracy of the Greenwald Algorithm

The microwave radiative transfer scheme obtained from C. Kummerow deals with transfer in a vertically inhomogeneous, non-isothermal plane parallel atmosphere. It accounts for thermal emission, absorption and multiple scattering by rain and ice. Although it uses the Eddington approximation, comparison with an 8-stream discrete ordinate scheme showed it to be accurate to within 1 to 2°C, under conditions appropriate to the simulation of SSM/I observations, (Kummerow, 1993). The key advantage of the Eddington scheme is its speed.

Kummerow's scheme requires as input, profiles of temperature, relative humidity, cloud water mixing ratio, rainfall rate and the equivalent rainfall rate of ice, plus surface wind speed and sea-surface temperature. No ice was included in the work described here.

The accuracy of the Greenwald algorithm was investigated using input data similar to that used by Prigent et al. (1994). The sea-surface temperature was 14°C, lapse rate 7°Ckm^{-1} and surface wind speed 7 ms^{-1}. The relative humidity profile was taken from the Cox model and the humidity was above 90% from the surface to 4 km. A

cloud of constant mixing ratio was inserted from 0 - 2 km and the mixing ratio varied to give LWP values in the range 0 - 3000 gm^{-2}. The Greenwald diagnosed LWP is plotted against the actual value in Figure 12a. The good agreement found by Penney (1994) is reproduced.The accuracy declines above about 1200 gm^{-2}. The test was repeated with the same inputs except that the cloud was inserted from 2 to 4 km (ie 0 to -12°C). The Greenwald estimate, shown in Figure 12b, is now slightly larger than the actual LWP but the accuracy is still good up to 1100 gm^{-2}, although the SSM/I signal saturates quickly at higher LWPs. The lack of sensitivity to the actual cloud temperature is encouraging for the use of the Greenwald algorithm. However, it also suggests that there is little information on the temperature of the cloud water in the SSM/I brightness temperatures.

Close examination of Fig 12 indicates a tendency for the Greenwald algorithm to overestimate, especially at the colder temperatures. This was found subsequently to be due to the Kummerow scheme producing brightness temperatures at 19V, 22V which appeared 4 - 5°C too cold. The main impact on the Greenwald algorithm was caused by the bias in the 19V temperature. For the clear sky case, the Greenwald algorithm fed with brightness temperatures from the Kummerow scheme, produced positive LWP values eg 38 gm^{-2} with a windspeed of 5 ms^{-1}. This is a larger bias than that produced by the clear sky brightness temperatures obtained from the radiative transfer scheme used by Penney (1994), which was less than 10 gm^{-2} at 5 ms^{-1}.

In the final series of tests, rainwater was inserted between 0 and 2 km, with no cloud water present. The rainfall rate, assumed constant with height, was varied from 0.1 to 20 mmh^{-1}, producing LWP values of 26 - 2200 gm^{-2}. The Greenwald estimates are shown plotted against the actual values in Figure 12c. It can be seen that the Greenwald algorithm overestimates for actual LWPs up to about 700 gm^{-2} (5 mmh^{-1}) and then progressively underestimates, presumably because of the effects of scattering. The apparent cold bias in the 19V, 22V brightness temperatures produced by the Kummerow scheme produces an overestimate of around 40 gm^{-2}, which only affects the results at low rainfall rates. At a true value of 500 gm^{-2}, the LWP is overestimated by 60% by the Greenwald algorithm. A mixture of cloud water and rain water also causes the Greenwald algorithm to overestimate. As will be illustrated later, the contribution of rain to the LWP in the cases studied is believed to be too low to explain the gap between the Greenwald estimate and the Cox model prediction.

Finally, it should be noted that Liu and Curry (1993) present arguments which raise a question mark over the applicability to the real atmosphere of a theoretical demonstration of overestimation when rain is present. The Liu and Curry (1993) algorithm for LWP does not account formally for rain. They have evaluated the error due to rain by comparison with a sophisticated radiative transfer scheme and found that there is overestimation by a factor of 2, up to 3000 gm^{-2} (eg for a cloud with an LWP of 500 gm^{-2} due to cloud water and 500 gm^{-2} due to rain, their algorithm gave 2000 gm^{-2}). However, the plane parallel atmosphere assumed by the radiative transfer schemes ignores the effect of variations in rainfall rate over the field of view of an SSM/I pixel. According to Liu and Curry (1993), the non-linear relationship between LWP and brightness temperature always produces an underestimate of LWP, when the LWP varies over an SSM/I pixel. They quote Chiu et al. (1990) who found that a plane parallel scheme would make a 50% underestimate of rainfall rate because of sub-pixel variations in rainfall rate. Liu and Curry (1993) assume that the same underestimation would occur due to sub-pixel variations in cloud LWP and rain LWP, for clouds with LWP above 500 gm^{-2}. This would offset their factor of 2 overestimation in a plane parallel atmosphere, leading to a reasonable answer. For clouds with LWP less than 500 gm^{-2} they assume that the relationship between LWP and brightness temperature is sufficiently linear to avoid a significant underestimation due to inhomogeneities.

6.2 Use of Brightness Temperatures Directly

Kummerow and Giglio (1994a,b) applied the Kummerow radiative transfer scheme to the retrieval of surface rainfall rate and cloud liquid water content. The method had some similarities to that used originally for satellite sounding, where the best match to an archive of soundings was made. They used 27 cloud structures defined by the liquid water content, rain water content and ice content in five layers, the actual values being defined by the surface rainfall rate. By varying the relevant parameters eg rainfall rate, cloud liquid water content, surface

temperature, linear regressions were produced between surface rainfall rate and SSM/I brightness temperatures calculated from the radiative transfer scheme. To retrieve surface rainfall rate, the observed brightness temperatures were fed into the regression relationship for each cloud structure to produce several estimates of surface rainfall. To choose the best solution, the radiative transfer code was applied to each cloud structure to calculate the brightness temperatures. The optimum solution was taken to be the one which minimised the difference between the simulated and observed brightness temperatures. Using radar data as ground truth, Kummerow and Giglio (1994a) showed that the error in retrieved surface rainfall rate decreased as the root mean square (RMS) difference between simulated and observed brightness temperatures decreased. RMS differences above 5°C indicated an unacceptable solution.

Prigent et al. (1994) retrieved rainfall rate, LWP and other parameters using a variational scheme in conjunction with a radiative transfer scheme. The optimum solution was obtained by minimising the difference between simulated and observed brightness temperatures, with due allowance for errors in the observations.

We have undertaken a limited study of the direct use of brightness temperatures, in particular to look at the sensitivity of the RMS difference between simulated and observed brightness temperatures as an indicator of the differences in LWP produced by the Cox model and mesoscale model. Point 2 from the 9 Nov. 93 case was studied initially, which is just west of the colder cloud and within the western band of larger LWP values. Profiles of temperature, relative humidity, LWC and rainfall rate were extracted from Cox model run 2 and used to run the Kummerow scheme. The LWC profile was then replaced with one from the mesoscale model, derived from Fig 11, in the region of the low-level LWC maximum west of Scotland. All other input profiles remained the same. The rain contributed 79 gm^{-2} to the LWP in both cases. The results are summarised in Table 5 which shows the observed and calculated brightness temperatures for each SSM/I channel and the RMS difference between the observed and calculated values. The actual LWP input to the Kummerow scheme (cloud plus rain) and the Greenwald estimate are also shown. The Cox model LWC profile produces brightness temperatures which are too cold, indicating insufficient liquid water and resulting in an RMS difference of 13°K. Use of the mesoscale model LWC profile produces brightness temperatures which are too warm, except at 19V, 22V. The RMS difference of 8°C is lower than produced by the Cox model LWCs, but still larger than the 5°C considered indicative of an acceptable solution by Kummerow and Giglio. The fourth row in Table 5 shows the results when the mesoscale model cloud LWCs are halved. The RMS difference is reduced to 2.6°C, within the acceptable range. Table 5 also shows that the Greenwald LWP derived from the observed brightness temperatures agrees best with LWP produced by halving the mesoscale model cloud LWCs.

Table 5 Observed and Simulated SSM/I Brightness Temperatures (°C)

SSM/I Channel	19H	19V	22V	37H	37V	85H	85V	RMS Diff. (°C)	Total LWP (gm^{-2})
Observed	144	197	220	188	225	259	263	-	340*
Cox LWC	136	189	211	171	217	245	259	13.0	104
Mesoscale LWC	151	198	219	203	235	266	269	8.0	539
Mesoscale LWC/2	144	194	215	188	227	259	266	2.6	309

* Greenwald estimate

Table 5 shows that for most SSM/I channels the difference between observed and calculated brightness temperatures for the last case was less than 2°C but the simulated temperatures were significantly colder for 22v (5°C) and 19V (3.5°C). The most likely explanation was felt to be a known problem with the gaseous absorption coefficients for water vapour and oxygen which are calculated from Liebe's model (Liebe, 1989) in the

Kummerow scheme. Following Prigent (1994), the water vapour absorption coefficients were increased by 8% for the lower three SSM/I channels. This resulted in a 1.5°C increase in the 19H, 22V brightness temperatures and a 1°C increase in the 19V brightness temperature, which only partially solves the problem. The sensitivity of the low frequency brightness temperatures to the relative humidity profile was also investigated, by increasing the relative humidities by 1%. This increased the 22V brightness temperature by 0.12°C and the 19V brightness temperature by 0.05°C. However, since the higher frequency brightness temperatures were increased by around 0.03°C, the relative increase at 22V is only around 0.09°C. A naive extrapolation of these results would suggest that an increase in relative humidity of 40% would be required to remove the 22V anomaly. However, the relative humidity fed into the Kummerow scheme was already above 95% to 3 km and only decreased to 89% at 8 km.

Encouraged by these results, a more formal iteration technique for use with the Kummerow scheme was developed. The iterative process starts with a low or zero rainfall rate and then increases the cloud LWP in small steps until a minimum in RMS difference is well defined. The rainfall rate is then increased and the cloud LWP iteration repeated. Finally, from the series of minima for each rainfall rate, the overall minimum is selected as the final solution . The method was applied to points 1 and 2, defined in Table 2. The temperature, relative humidity and rainfall rate profiles were taken from the Cox model runs for these points. The liquid water content profile was taken from the mesoscale model cross section at 57°N. The SST was 282.4°C and the surface wind speed 12 ms^{-1}.

Initial attempts at iteration produced rather flat minima, the reason being that the bias in 19V, 22V brightness temperatures caused these channels to dominate the RMS difference near the minima. The iterations were repeated with 3.5°C added to 19V and 3°C added to 22V brightness temperatures from the Kummerow scheme. They were also repeated with these channels excluded. The results were similar in both cases and resulted in a sharpening of the minima, although there are minor oscillations as the minima are approached. The results with the bias corrected are shown for points 1 and 2 are in Figures 13a, 13b. Each point represents the minimum RMS difference for a given surface rainfall rate. The LWP through the rain and cloud are plotted separately against RMS difference and the combined LWP is also plotted. For example, on Fig 13a, an RMS difference of around 3.7°C is associated with a cloud LWP of 56 gm^{-2}, a rain LWP of 158 gm^{-2} and hence a total LWP of 214 gm^{-2}. When the rain contribution is decreased to 142 gm^{-2}, a minimum RMS difference of 3.0°C is achieved with a cloud LWP of 81 gm^{-2}.

Figure 13 shows that for point 1 the minimum occurs with a total LWP around 310 - 340 gm^{-2} and around 335 - 370 gm^{-2} for point 2. The Greenwald estimates for these points are 325 gm^{-2} and 340 gm^{-2} respectively. Both points analysed indicate that the Greenwald algorithm is providing a good estimate of LWP. The reason appears to be that the LWP due to rain is sufficiently low for the algorithm to give a reasonable estimate of its magnitude. (The rainfall rates at the minima are 0.5 mmh^{-1} at point 1 and 0.8 mmh^{-1} at point 2). Figure 12c indicates that this is unlikely to be true for much larger rain contributions. Also, the LWP due to rain contributes a third or less to the total at these two points.

Although the accuracy of the Greenwald technique was confirmed for the two points studied, minimization of the difference between the observed and simulated brightness temperatures has two important advantages over the use of an algorithm. An indication of the accuracy of the estimated LWP is provided and there is some sensitivity to the relative contribution of cloud water and rain water. The latter property should allow some unrealistic Cox model solutions to be detected eg with spuriously high rainfall rates. The technique can also cope with rain and ice. Although the Kummerow scheme allows the input of an ice profile, this was not attempted here. It would be relatively easy to input such a profile from the Cox or mesoscale models. Whether it would be necessary to iterate with respect to the ice profile, or whether it could be tied to the rain profile remains to be investigated.

A disadvantage of the iterative approach is the computational burden of running a radiative transfer scheme

several times for each pixel. However, the Kummerow scheme only take 1 - 2 s on an Alpha workstation. Another disadvantage is that a more complete description of the atmosphere is necessary than is required by an algorithm. If the Kummerow scheme is used, then some correction has to be applied to the 19V, 22V channels, or they have to be ignored.

It should be noted that two corrections applied by Kummerow and Giglio (1994b) to the SSM/I data were not applied here. To allow for the variation of the SSM/I footprint with frequency, they normalised all channels to the 37 GHz footprint. A correction was also applied for the variability of rainfall rate within a footprint. The variance of the rainfall rate field within each pixel was estimated from the 85 GHz data in the surrounding pixels. A mean brightness temperature was then calculated by integrating over a lognormal distribution with the assumed mean rate and estimated variance. This required the Kummerow scheme to be run 100 times for each iteration in estimated mean rainfall rate. Such corrections were not used by Prigent (1994) and despite not using them here, it was possible to achieve excellent agreement with the observed brightness temperatures. This is presumably because we are dealing with a stratiform case with low, relatively uniform rainfall rates. However, they could be necessary for global application where it would be necessary to deal with convection.

The most significant conclusion reached from the investigations with the Kummerow scheme is that the problem of matching Cox model and SSM/I LWP estimates is mainly due to the Cox model solution in the frontal cases studied.

7. Discussion and Conclusions

This study has concentrated upon cyclonic systems because, although stratocumulus and stratus are common over the oceans they are predominantly above 0°C, except at high latitudes. Also, the ability of microwave techniques to retrieve LWP in simple layer clouds composed primarily of water has been demonstrated, (English, 1996, Cober et al., 1996). Any climatology of supercooled water has to encompass cyclonic systems, where the cloud will extend to temperatures well below freezing in most cases. The presence of rain and ice complicates the interpretation of SSM/I data in such systems. The process of glaciation becomes the central issue in determining the occurrence of supercooled liquid water.

The proposed development of a climatology of supercooled liquid water contents based on LWP diagnosed from SSM/I data has not proceeded, because of problems with the method used to distribute the liquid water in the vertical. This involves running a 2-D cloud model, the Cox model, with various vertical velocities until it produces an LWP in agreement with the SSM/I estimate. The liquid water contents can then be extracted from the model as a function of temperature and altitude. The key problem has been the inability of the Cox model to produce LWP values as large as those inferred from the SSM/I data. Our studies, although limited, found that mesoscale areas with LWP around 300 - 500 gm^{-2} were commonly associated with cyclonic systems. The Cox model could only produce such values easily when cloud first formed. The formation of precipitation led to a marked reduction in LWP because of the removal of supercooled water by glaciation and the washout of warm cloud water by rain. This made it difficult to generate LWP values due to cloud in excess of 100 - 200 gm^{-2}, except near the upwind cloud edge, where precipitation had not had time to form. To produce the typical SSM/I values it was necessary to increase the vertical velocity so that rain made the major contribution to the total LWP. However, this model solution has been called into question by using a radiative transfer scheme which can account for the effects of rain, to simulate SSM/I brightness temperatures. By adjusting the relative amounts of rain and cloud water, the difference between the simulated and observed brightness temperatures for the 9 Nov. 93 case was minimised for pixels exhibiting a large LWP value, when cloud water contributed two thirds of the total LWP and rain water one third. Although the technique was only applied to a few pixels, this result is in agreement with a mesoscale model forecast from a new version of the model containing an explicit microphysics scheme, similar to the Cox model scheme. In the mesoscale model forecast, cloud water at temperatures above 0°C made the major contribution to the LWP. Aircraft LWC profiles from the CASP II

project area, which generally terminated several hundred metres above the surface, also implied most LWP values due to cloud were less than 200 gm^{-2}. If rain were making a minor contribution then there must be a significant contribution to the LWP from low-level cloud. However, CASP II profiles obtained on take off and landing did not have larger LWPs. Perhaps they were in a less active part of the system. It is clear that further in-situ measurements are required to determine the relative contributions of cloud water above 0°C, cloud water below 0°C and rain to the total LWP, particularly where large values are diagnosed from SSM/I data.

Both the Greenwald algorithm, used to infer LWP from the SSM/I brightness temperatures and the Cox model have been investigated to try and resolve the discrepancy. The Greenwald algorithm had already been demonstrated theoretically to have an RMS error around 40 gm^{-2} for layer clouds without precipitation or ice. It has been shown here that the Greenwald algorithm overestimates the LWP due to rain, the error increasing with rain rate to a maximum around 60% at 500 gm^{-2}. However, the cases studied here probably had sufficiently low rain LWP values to allow the Greenwald algorithm to give a good estimate. The technique of adjusting the rain and cloud LWP iteratively, in order to minimize the difference between observed brightness temperatures and those simulated with the Kummerow radiative transfer scheme is recommended. Although this uses more CPU, time it has several advantages over use of an algorithm. It can cope with rain and ice and appears to quantify the relative contribution of rain and cloud to the LWP. It also gives an indication of the quality of the final solution from the RMS difference between the observed and simulated brightness temperatures. Before the technique can be applied globally, the effects of variations in rainfall rate across the footprint and the mismatch in footprint size at different frequencies have to be addressed, following Kummerow and Giglio (1994). The possibility of an emission analogue of the radar bright-band effect due to melting snowflakes should also be considered.

The failure of the Cox model to produce LWP values as large as inferred from the SSM/I data probably has several causes. The mesoscale model results for the 9 Nov. 93 case and the CASP II aircraft data suggest that a major contribution to LWP comes from cloud near the surface. The Cox model does not contain a boundary layer mixing scheme and so cannot generate stratocumulus and stratus cloud by the appropriate physical process. All low-level cloud in the Cox model is generated by steady ascent. A related problem is that the vertical velocity profile had to be prescribed in the Cox model and this was poorly defined because archived values were only available at four heights. The mesoscale model produced a low-level peak on 9 Nov. 93 which was not resolved by the archived vertical velocities. This helped the mesoscale model produce a larger LWC value than the Cox model, although it was of secondary importance to the effect of cloud top height, described below. Tests with the Cox model found that the results are only sensitive to the height of the vertical velocity peak when this approaches the freezing level. However, a broad vertical velocity profile will produce a higher LWP than a narrow profile with the same peak value.

The Cox model has been integrated to steady state with a constant, horizontally uniform, vertical velocity profile. However, it is likely that most supercooled liquid water is associated with embedded (upright) convection or regions of enhanced ascent associated with slantwise instability, (Bohorquez and McCann, 1995). Thus, in reality the vertical velocity will vary spatially and temporarily. It is not clear that embedded convection can explain the widespread areas of large LWP values inferred from the SSM/I data, boundary layer cloud would seem a more likely cause.

Although the Cox model is no longer the state of the art model that it was when published, the results from it agree with current knowledge of the occurrence of supercooled water. In particular, supercooled water in the model was confined to temperatures warmer than -15 to -20°C, except when cloud first formed or when embedded convection was simulated. It also produced larger supercooled liquid water contents and higher LWPs as the cloud top temperature approached within 5°C of zero, because of the low concentration of ice nuclei assumed at these temperatures. However, for 9 Nov. 93 case the model failed to reproduce the warmer cloud top observed and associated large LWP values, unlike the mesoscale model. This may have been because of an error in the archived relative humidity profile from the Unified Model, used to run the Cox model. It may also be a

symptom of a failure to represent the 3-D airflow with the 2-D Cox model. It is likely that on 9 Nov. 93, relative to the system, the dry air aloft was being advected at 90° to the front, while the air at lower levels was moving along the front.

The main conclusions of the study may be summarised as follows.

• The Greenwald algorithm is likely to overestimate the LWP derived from SSM/I brightness temperatures when a significant contribution is made by rain, but appears sufficiently accurate for non-precipitating clouds.

• Retrieval of LWP by minimising the difference between observed and simulated brightness temperatures has the advantage of indicating the relative contributions of rain and cloud to the LWP, but uses more computer time and requires further development locally. It is recommended as the best approach for future global use.

• The LWP field diagnosed from the SSM/I data may be poorly correlated with the field of supercooled liquid water contents. Further observations are required to examine this issue.

• The Cox cloud model underestimates the LWP for all or some of the following reasons :-

(i) Errors in the initial conditions may produce an error in cloud depth.

(ii) The atmosphere rarely attains the steady produced by integrating the Cox model to equilibrium.

(iii) A significant fraction of the diagnosed LWP may be due to boundary layer cloud, whose development is not described properly by the Cox model.

• The cloud-top temperature and history of the cloud are important in determining supercooled liquid water contents.

• One aspect which should be studied more formally is the sensitivity of the diagnosed LWC profile, for a given LWP value, to the history of the cloud. If little sensitivity was found this would mitigate some of the problems with the technique.

Acknowledgements

The work was funded by the Safety Regulation Group of the Civil Aviation Authority under contract number 7D/S/1260/1.We also wish to thank the following for their assistance. The CASP II aircraft data were provided by Dr. G. Isaac and W. Strapp of the Atmospheric Environment Service, Canada and the CASP II liquid water content climatology by W. G. Tank of the Boeing Defense and Space Group, Seattle. G. Penney provided the coded LWP algorithms and the SSM/I data processing software. S. Ballard provided the results from the mesoscale model. Dr.D. Jones and Dr. S. English assisted us with the use of the radiative transfer code which was provided by Dr. C. Kummerow.

References

Ballard, S. P. and M. G. Hutchinson, 1995: Parametrization of mixed-phase cloud and precipitation. Joint Centre for Mesoscale Meteorology, Reading, England, Internal Report 48.

Bohorquez M. A. and D. W. McCann, 1995: Model proximity soundings near significant aircraft icing reports. Proc.Sixth Conf. on Aviation Weather Systems, Dallas, Texas, Amer. Meteor. Soc., Boston, 249 - 252.

Browning, K. A. and G. A. Monk, 1982: A simple model for analysis of cold fronts. Q. J. R. Meteorol. Soc., 108, 435 - 452.

Chiu, L. S., G. R. North, D. A. Short and A. McConnell, 1990: Rain estimation from satellites: Effect of finite field of view. J. Geophys. Res., 95, 2177 - 2185.

Cober, S. G., G. A. Isaac and J. W. Strapp, 1995: Aircraft icing measurements in East Coast winter storms. J. Appl. Met., 34, 88 - 100.

Cober, S. G., A. Tremblay and G. A. Isaac, 1996: Comparisons of SSM/I liquid water paths with aircraft measurements. J. Appl. Met., 35, 503 - 519.

Cox, G. P., 1988: Modelling precipitation in frontal rainbands. Q. J. R. Meteorol. Soc., 114, 115 - 127.

Cullen, M. J. P., 1993: The Unified Forecast/Climate model. Meteorol. Mag., 122, 81 - 94.

Curry, J. A. and G. Liu, 1992: Assessment of aircraft icing potential using satellite data. J. Appl. Met., 31, 605 - 621.

English, S. J., 1991: Remote sensing of meteorological parameters by microwave radiometry. Ph.D. Thesis, St. Cross College, Oxford University.

English, S. J., 1995: Airborne radiometric observations of cloud liquid-water emission at 89 and 157 GHz: Application to retrieval of liquid-water path. Quart. J. Roy. Met. Soc., 121, 1501 - 1524.

Greenwald, T. J., G. L. Stephens, T. H. Vonder Haar and D. L. Jackson, 1993: A physical retrieval of cloud liquid water over the global oceans using Special Sensor Microwave/ Imager (SSM/I) Observations. J. Geophys. Res., 98, 18471 - 18488.

Grody, N. C. and R. R. Ferraro, 1992: A comparison of passive microwave rainfall retrieval techniques. Proc. Sixth Conference on Meteorology and Oceanography, AMS, Atlanta, GA, 60 - 65.
Heymsfield, A. J., 1977: Precipitation development in stratiform ice clouds: A microphysical and dynamical study. J. Atmos. Sci., 34, 367 - 381.

Jeck, R. K., 1983: A new data base of supercooled cloud variables for altitudes up to 10,000 feet AGL and the implications for low altitude aircraft icing. U.S. Dep. Transport Rep. DOT/FAA/CT-83/21.

Karstens, U., C. Simmer and E. Ruprecht, 1994: Remote sensing of cloud liquid water, Meteorology and Atmos. Phys., 54, 157 - 171.

Kummerow, C., 1993: On the accuracy of the Eddington approximation for radiative transfer in the microwave frequencies. J. Geophys. Res., 98, 2757 - 2765.

Kummerow, C., R. A. Mack and I. M. Hakkarinen, 1989: A self-consistency approach to improve microwave rainfall rate estimation from space. J. Appl. Met., 28, 869 - 884.

Kummerow, C. and L. Giglio, 1994a: A passive microwave technique for estimating rainfall and vertical structure information from space. Part 1: Algorithm description. J. Appl. Met., 33, 3 - 18.

Kummerow, C. and L. Giglio, 1994b: A passive microwave technique for estimating rainfall and vertical structure information from space. Part 2: Application to SSM/I data. J. Appl. Met., 33, 19 - 34.

Liebe, H. J., 1989: MPM - an atmospheric millimetre-wave propagation model. Int. J. Infrared and Millimetre Waves, 10, 6, 631 - 650.

Lin, B. and W. B. Rossow, 1994: Observations of cloud liquid water path over oceans: Optical and microwave remote sensing methods. J. Geophys. Res., 99, 20,907 - 20,927.

Liu, G. and J. A. Curry, 1992: Retrieval of precipitation from satellite microwave measurement using both emission and scattering. J. Geophys. Res., 97, 9959 - 9974.

Liu, G. and J. A. Curry, 1993: Determination of characteristic features of cloud liquid water from satellite microwave measurements. J. Geophys. Res., 98, 5069 - 5092.

Liu, G. and J. A. Curry, 1995: Cloud properties over winter North Atlantic and Arctic Oceans as inferred from satellite data. Preprints Conf. Cloud Phys., Amer. Meteor. Soc., Boston, (J10) 12 - (J10) 15.

Lunnon, R. W., 1993: Project Definition Study of Icing Atmosphere for Aircraft Design. Forecasting Research Division, Tech. Rep. No. 57.

Penney, G. P., 1994: A sensitivity study of SSM/I statistical and physical liquid water path algorithms using a radiative transfer model. Forecasting Research Division, Tech. Rep. No. 110.

Prigent, C., A. Sand, C. Klapisz and Y. Lemaitre, 1994: Physical retrieval of liquid water contents in a North Atlantic cyclone using SSM/I data. Quart. J. Roy. Met. Soc., 120, 1179 - 1207.

Rutledge, S. A. and P. V. Hobbs, 1983: The mesoscale and microscale structure and organization of clouds and precipitation in midlatitude cyclones. VIII: A model for the "seeder -feeder" process in warm-frontal rainbands. J. A. S., 40, 1185 - 1206.

Rutledge, S. A. and P. V. Hobbs, 1984: The mesoscale and microscale structure and organization of clouds and precipitation in midlatitude cyclones. XII: A diagnostic modelling study of precipitation development in narrow cold-frontal rainbands. J. A. S., 41, 2949 - 2972.

Skatskii, V. I., 1965: Some results from experimental study of the liquid water content in cumulus clouds. Iz. Atmos. Oceanic Phys., 1, 479 - 487.

Takeda T. and G. Liu, 1987: Estimation of atmospheric liquid water amount by Nimbus 7 SMMR data: A new method and its application to the western North-Pacific region. J. Meteorol. Soc. Japan, 65, 931 - 946.

Warner, J., 1970: On steady-state one-dimensional models of cumulus convection. J. Atmos. Sci., 27, 1035 - 1050.

Zawadzki I., L. Ostiguy and J. P. R. Laprise, 1993: Retrieval of the microphysical properties in a CASP storm by integration of a numerical kinematic model. Atmos.-Ocean, 31, 201 - 233.

Figure Legend

Figure 1. Location of the fronts south of Newfoundland at 00 UTC on 5 Feb. 1992. The dashed line shows the track of the CASP II flight. SSM/I LWP values greater than 100 gm^{-2} in the vicinity of the fronts are contained within the dotted area.

Figure 2. SSM/I derived LWP values along two lines roughly perpendicular to the fronts in Figure 1.

Figure 3. Profiles of temperature, relative humidity, horizontal and vertical wind speed from 41.5°N, 54°W, used to initialize the Cox model to simulate the 5 Feb. 1992 CASP II case.

Figure 4. Results from the Cox model initialised with the profiles in Figure 3. (a) Cross section of cloud liquid water mixing ratio in gKg^{-1}. (b) Cross section of ice/snow mixing ration in gKg^{-1}. (c) Rainfall rate vs distance.

Figure 5. Liquid water path vs distance from the Cox model simulations of the 5 Feb. 1992 CASP II case. ---------- LWP due to cloud water $>$ 0°C. ..... LWP due to cloud water $\leq$ 0°C. - - - - - - - Total LWP due to cloud water. - - - - - - - LWP due to cloud water and rain water combined.

Figure 6. Profiles of cloud liquid water content vs height. (a) Measured during the aircraft descent in the warm sector on 5 Feb. 1992. (b) From the Cox model, 60 km from the upstream boundary. (c) As (b) but at 120 km. (d) As (b) but at 160 km.

Figure 7. As Fig. 6 but with LWC plotted against temperature.

Figure 8. Meteosat infrared image for 9 Nov. 1993 at 1830 UTC. The location of the fronts is also marked.

Figure 9. SSM/I diagnosed LWP field for 9 Nov. 1993 at 1946 UTC. Some smoothing has been applied.

Figure 10. Liquid water path and ice water path from the 36-hour mesoscale model forecast for 18 UTC on 9 Nov. 1993. (a) LWP due to cloud water. (b) LWP due to cloud water $\leq$ 0°C. (c) LWP due to cloud water $>$ 0°C. (d) Ice/snow water path.

Figure 11. Cross sections from the 36-hour mesoscale model forecast for 18 UTC on 9 Nov. 1993. (a) Ice/snow mixing ratio in $KgKg^{-1}$. (b) Cloud liquid water mixing ratio in $KgKg^{-1}$. The freezing level is shown as a dashed line on (b).

Figure 12. Greenwald algorithm LWP, derived from simulated brightness temperatures vs true LWP. (a) For cloud water occupying the temperature range 11 to 0°C. (b) For cloud water occupying the temperature range 0 to -12°C. (c) For rainwater.

Figure 13. Root mean square difference between simulated and observed brightness temperatures for 9 Nov. 1993 case. (a) Point 1 (defined in Table 1). (b) Point 2. The LWPs due to cloud and rain are plotted separately and the total LWP is also plotted.

Figure 1

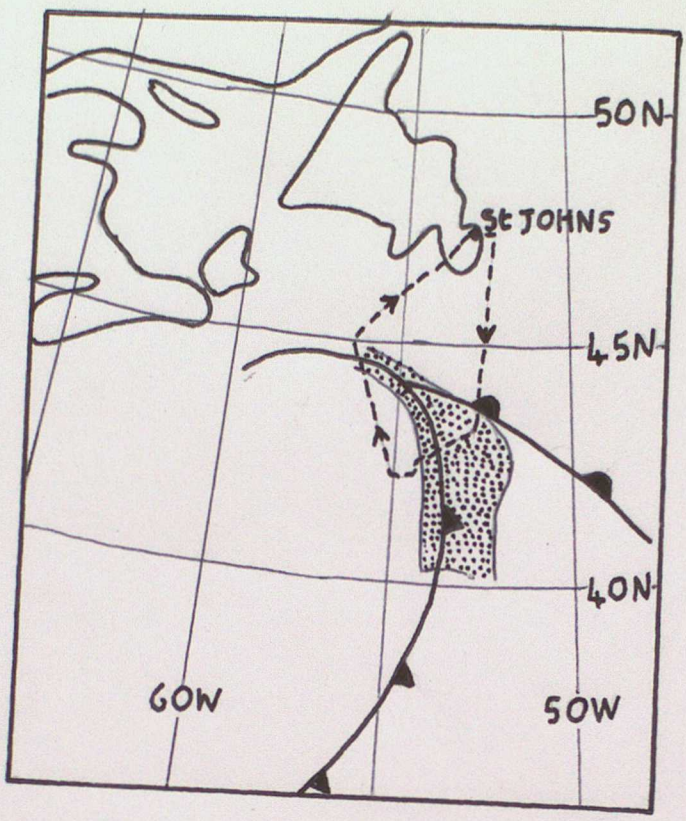
50N
St JOHNS
45N
40N
60W
50W

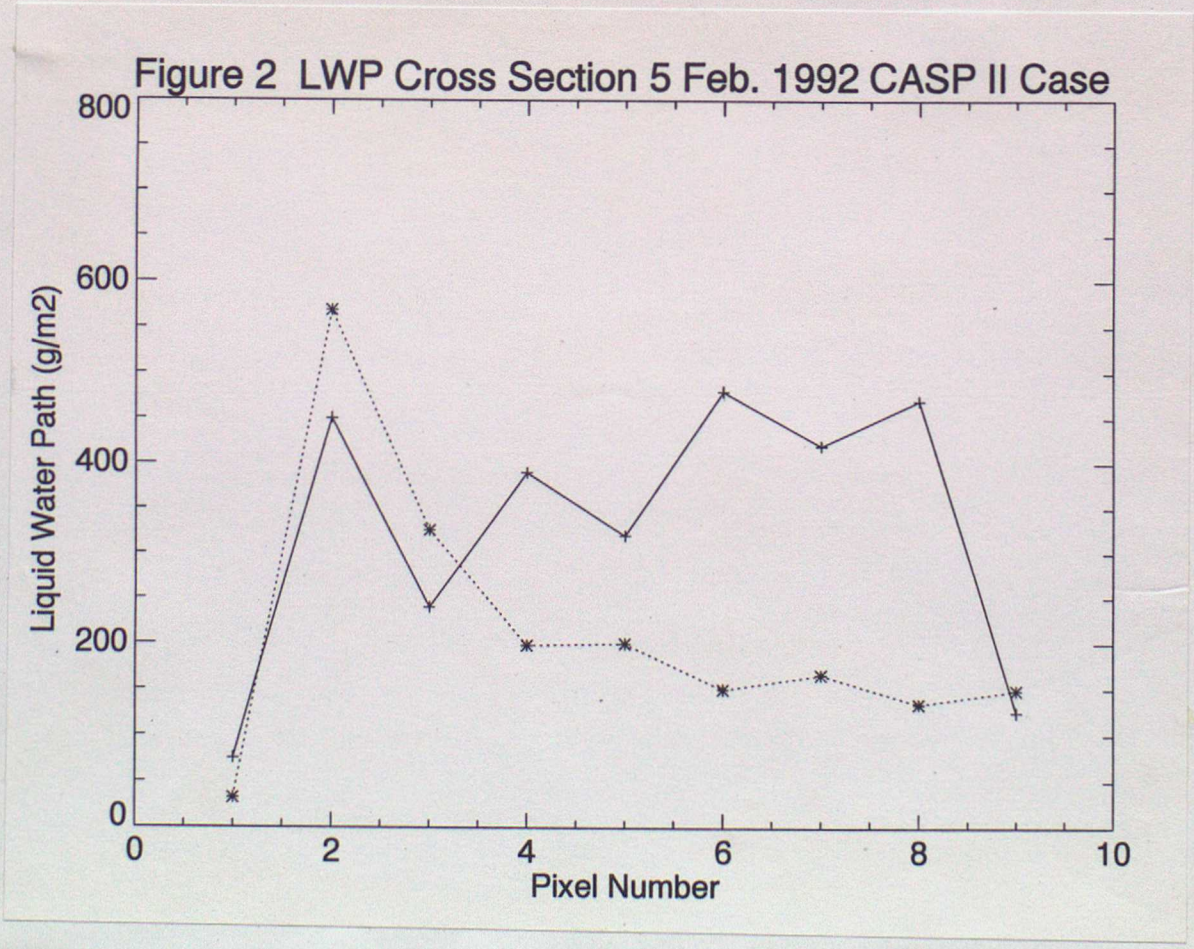
Figure 2 LWP Cross Section 5 Feb. 1992 CASP II Case
Liquid Water Path (g/m2)
800
600
400
200
0
0
2
4
6
8
10
Pixel Number

Figure 3

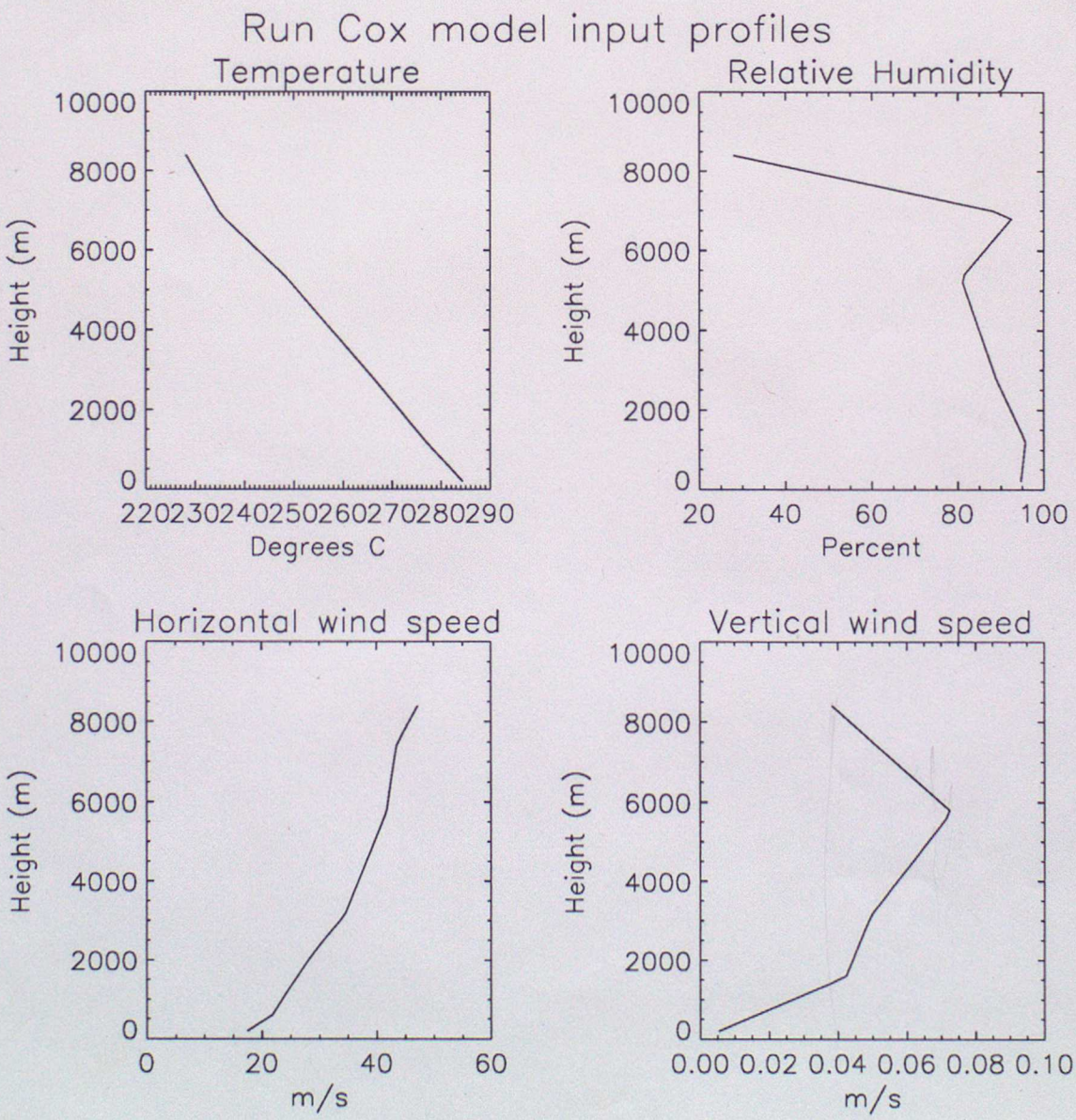
Run Cox model input profiles
Temperature
Relative Humidity
Horizontal wind speed
Vertical wind speed
Height (m)
10000
8000
6000
4000
2000
0
220230240250260270280290
Degrees C
20
40
60
80
100
Percent
0
20
40
60
m/s
0.00 0.02 0.04 0.06 0.08 0.10
m/s

Figure 4

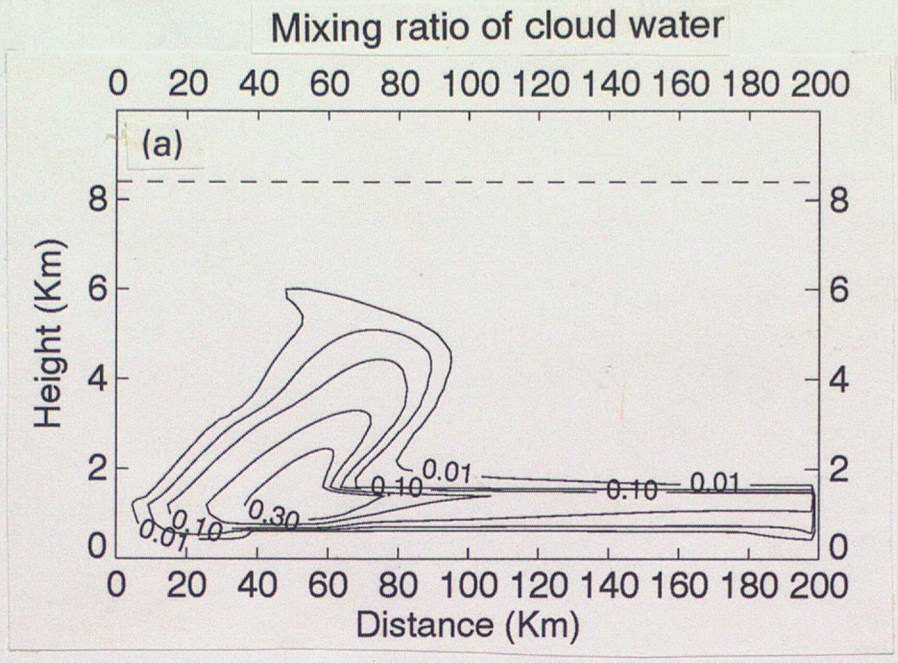
Mixing ratio of cloud water
(a)
Height (Km)
Distance (Km)
0 20 40 60 80 100 120 140 160 180 200
0 2 4 6 8
0.01
0.10
0.30
0.01
0.10
0.10
0.01

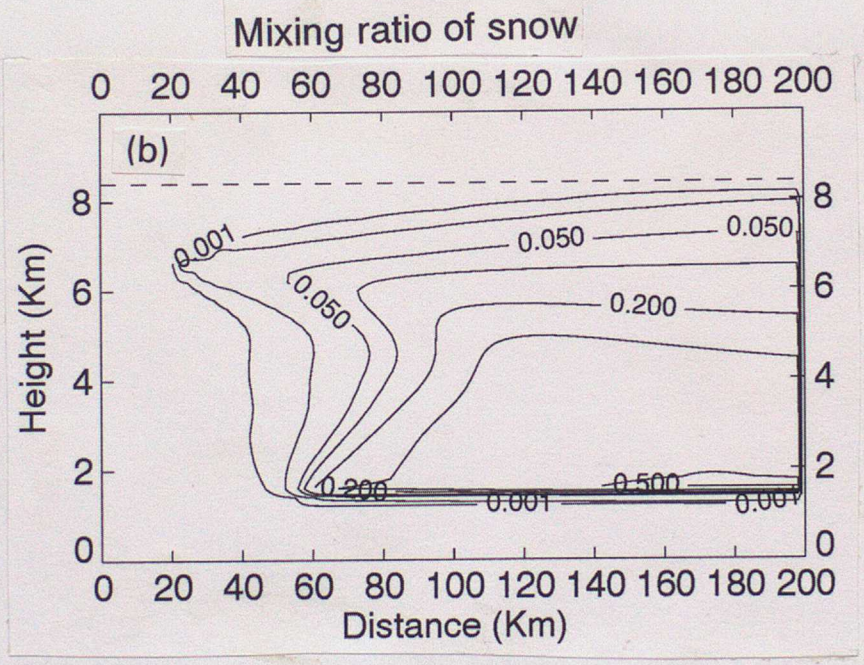
Mixing ratio of snow
(b)
Height (Km)
Distance (Km)
0 20 40 60 80 100 120 140 160 180 200
0 2 4 6 8
0.001
0.050
0.050
0.050
0.200
0.200
0.500
0.001
0.001

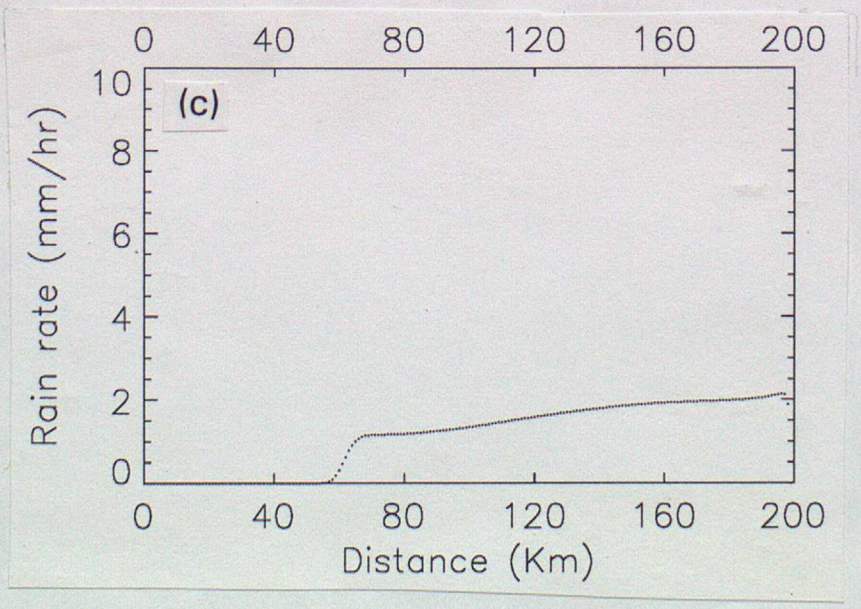
(c)
Rain rate (mm/hr)
Distance (Km)
0 40 80 120 160 200
0 2 4 6 8 10

Figure 5

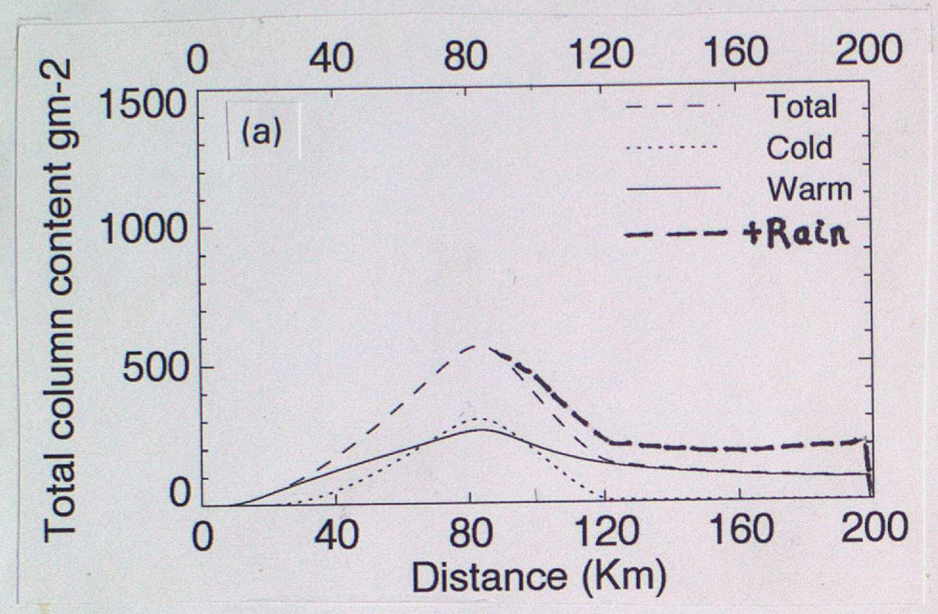
(a)
Total
Cold
Warm
+Rain
Total column content gm-2
Distance (Km)
0
40
80
120
160
200
500
1000
1500

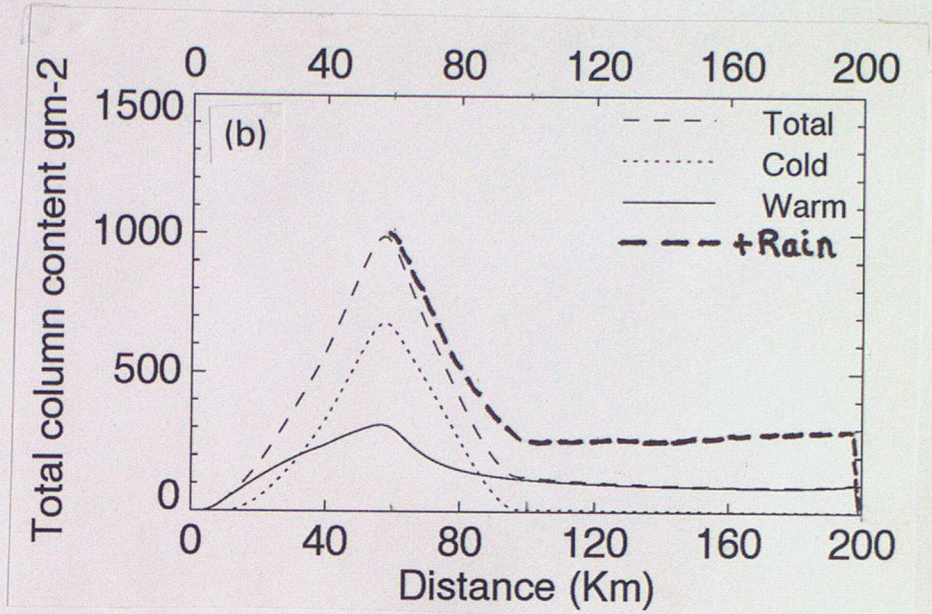
(b)
Total
Cold
Warm
+Rain
Total column content gm-2
Distance (Km)
0
40
80
120
160
200
500
1000
1500

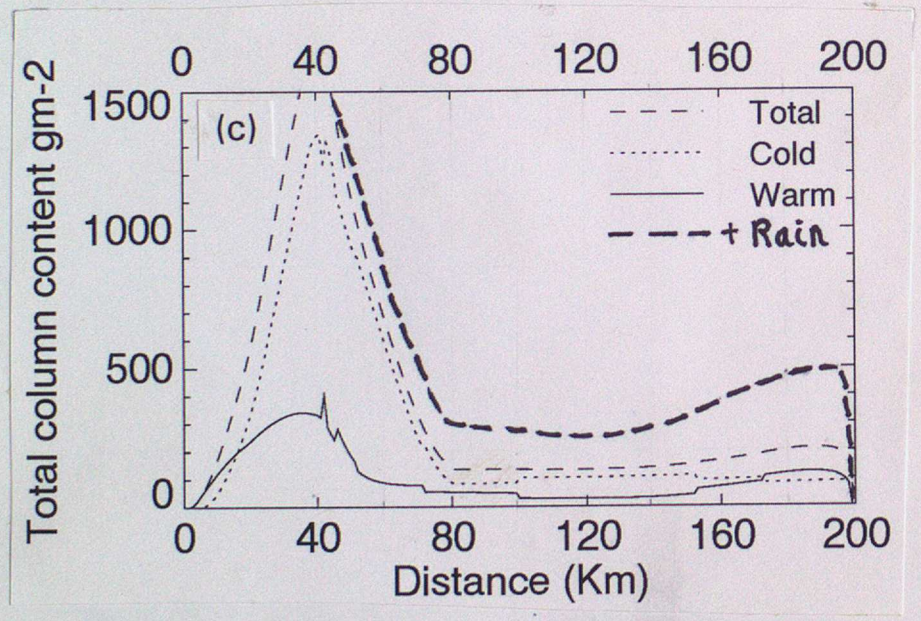
(c)
Total
Cold
Warm
+Rain
Total column content gm-2
Distance (Km)
0
40
80
120
160
200
500
1000
1500

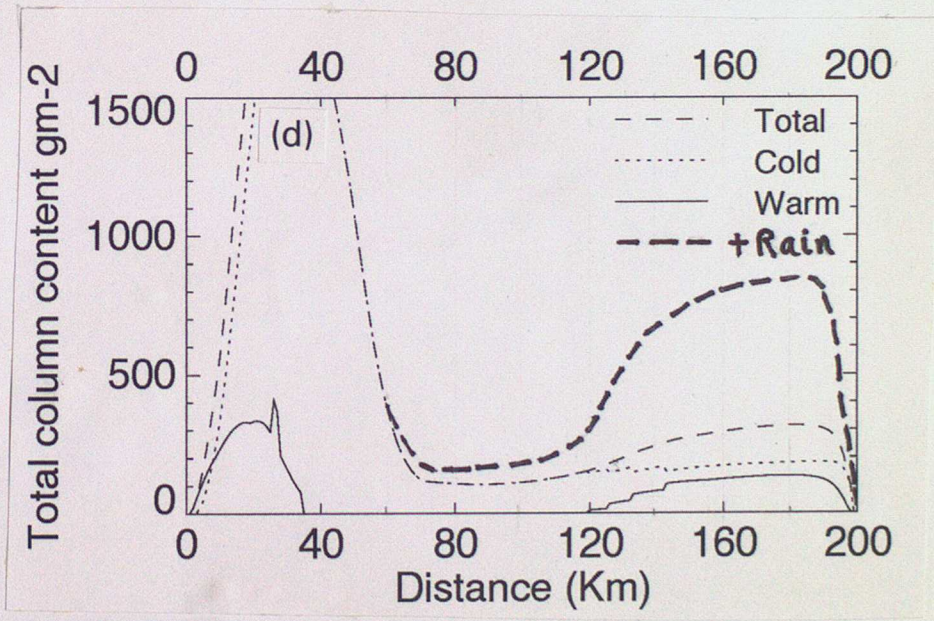
(d)
Total
Cold
Warm
+Rain
Total column content gm-2
Distance (Km)
0
40
80
120
160
200
500
1000
1500

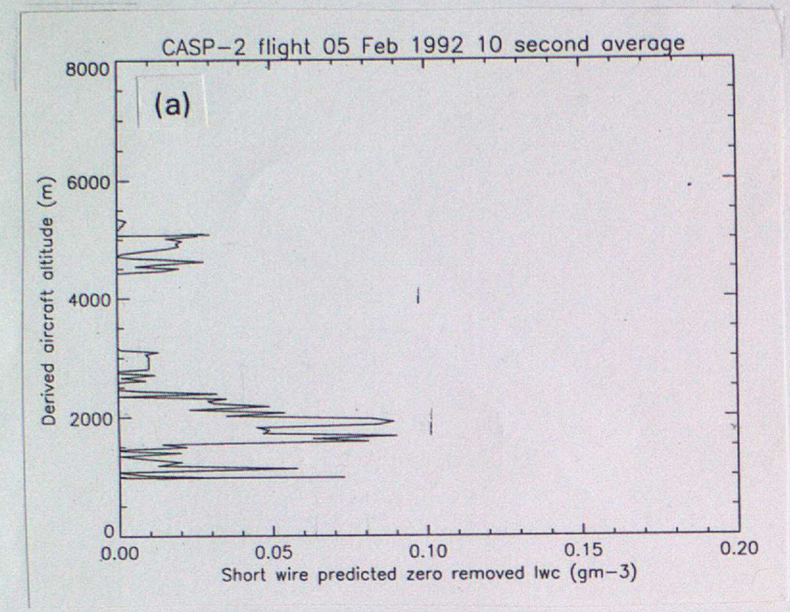
CASP-2 flight 05 Feb 1992 10 second average
(a)
Derived aircraft altitude (m)
8000
6000
4000
2000
0
0.00
0.05
0.10
0.15
0.20
Short wire predicted zero removed lwc (gm-3)

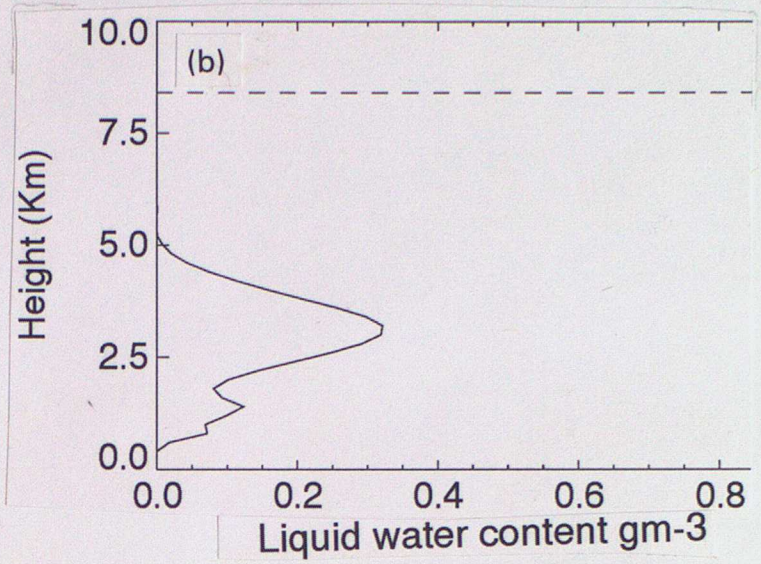
(b)
Height (Km)
10.0
7.5
5.0
2.5
0.0
0.0
0.2
0.4
0.6
0.8
Liquid water content gm-3

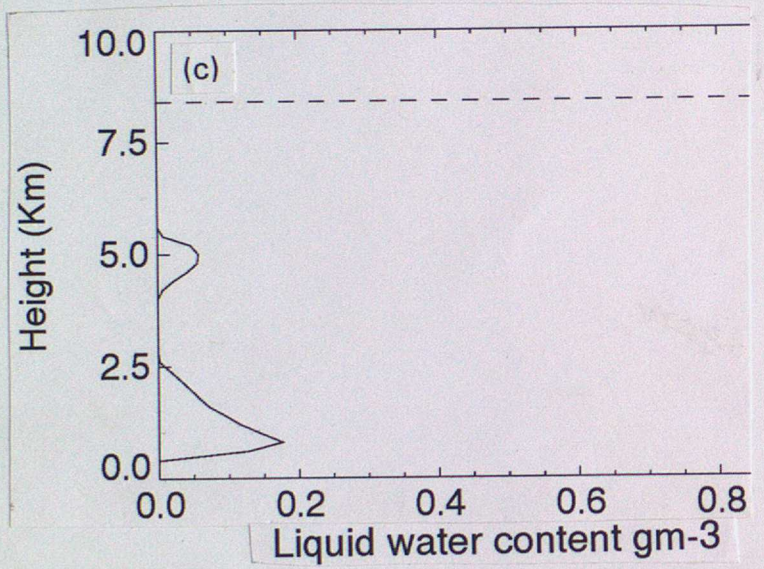
(c)
Height (Km)
10.0
7.5
5.0
2.5
0.0
0.0
0.2
0.4
0.6
0.8
Liquid water content gm-3

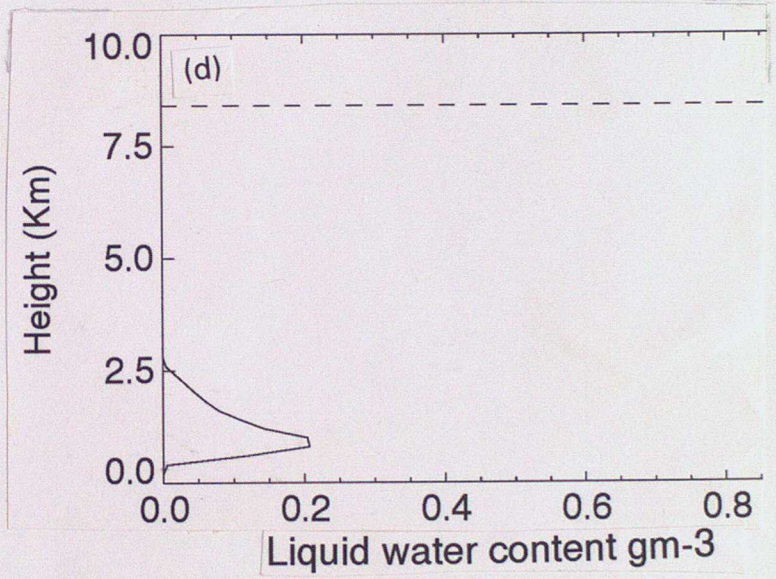
(d)
Height (Km)
10.0
7.5
5.0
2.5
0.0
0.0
0.2
0.4
0.6
0.8
Liquid water content gm-3

Figure 6

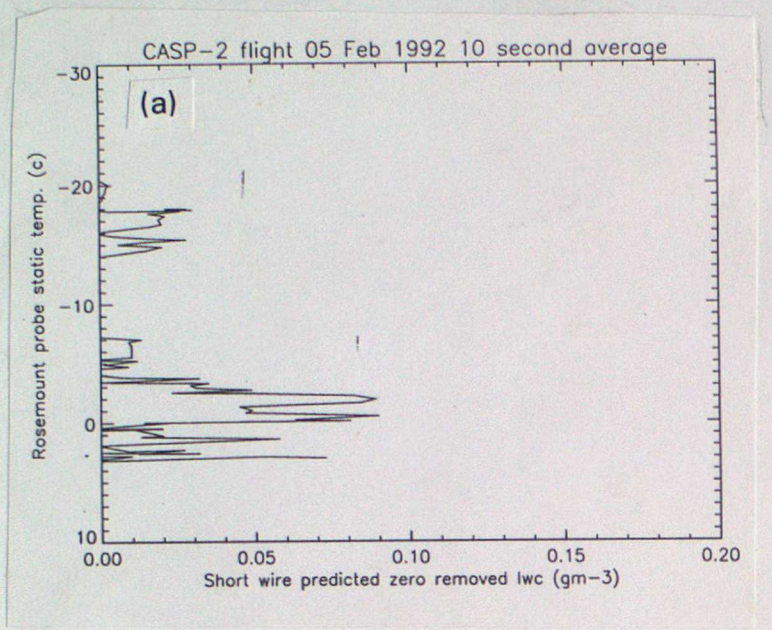
CASP-2 flight 05 Feb 1992 10 second average
(a)
Rosemount probe static temp. (c)
-30
-20
-10
0
10
0.00
0.05
0.10
0.15
0.20
Short wire predicted zero removed lwc (gm-3)

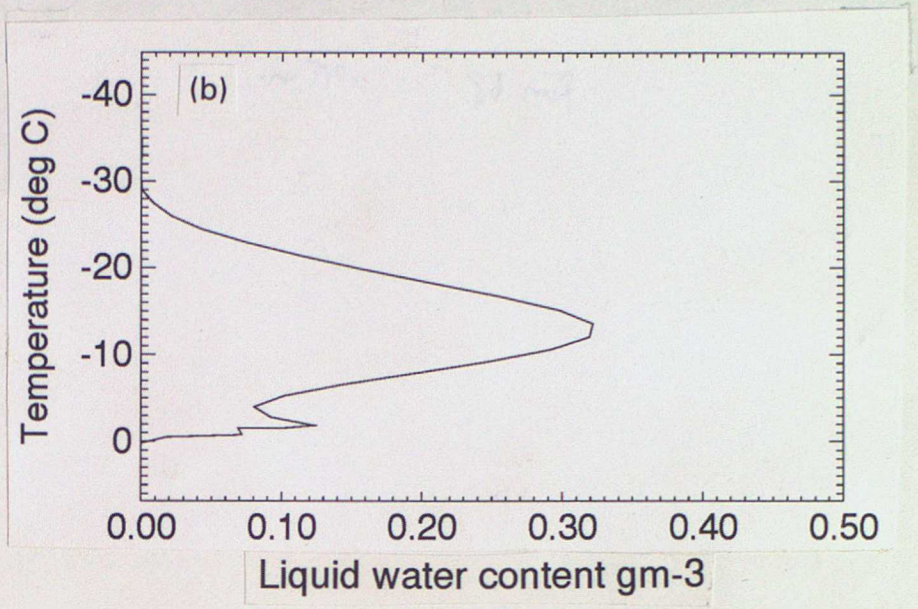
(b)
Temperature (deg C)
-40
-30
-20
-10
0
0.00
0.10
0.20
0.30
0.40
0.50
Liquid water content gm-3

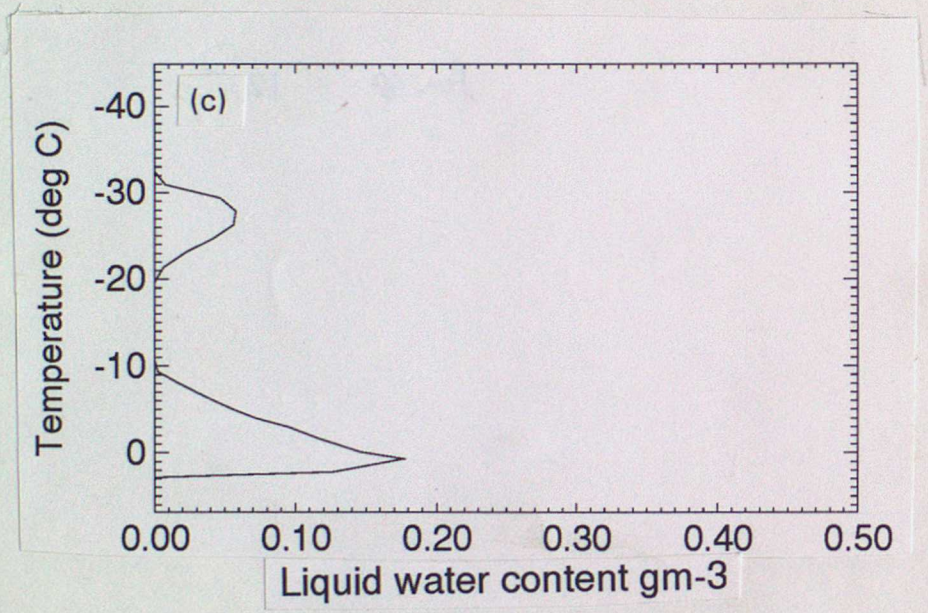
(c)
Temperature (deg C)
-40
-30
-20
-10
0
0.00
0.10
0.20
0.30
0.40
0.50
Liquid water content gm-3

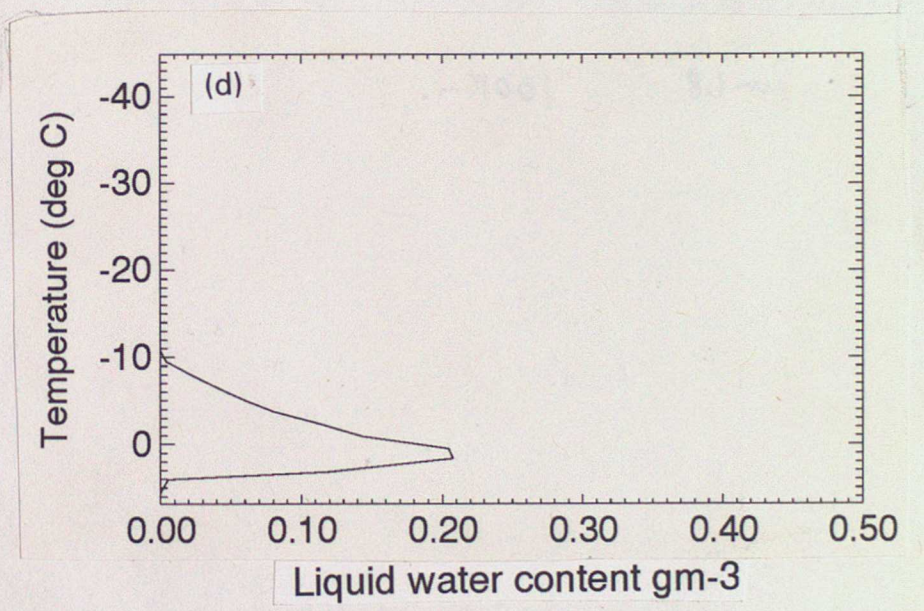
(d)
Temperature (deg C)
-40
-30
-20
-10
0
0.00
0.10
0.20
0.30
0.40
0.50
Liquid water content gm-3

Figure 7

Figure 8

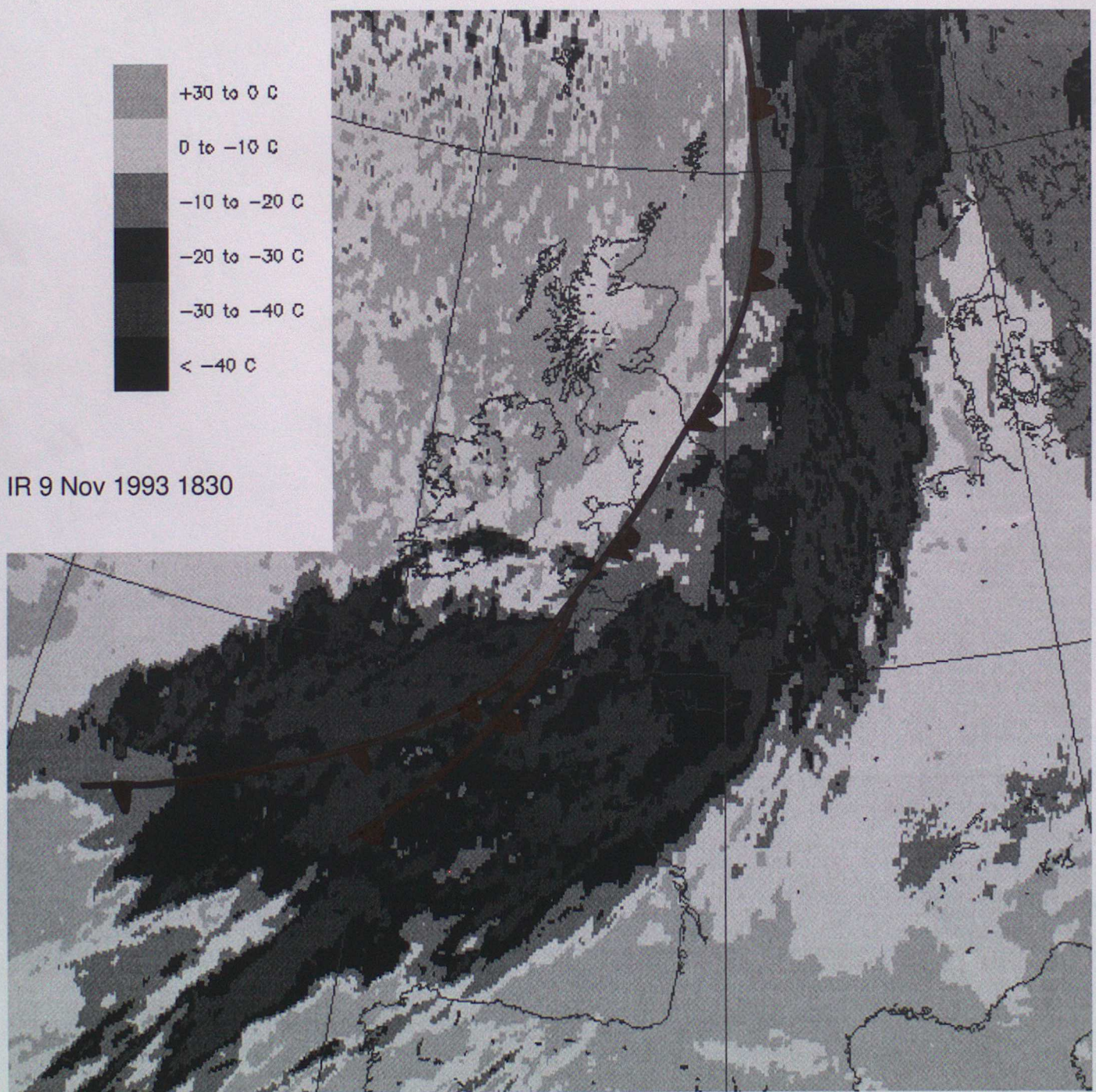
+30 to 0 C
0 to −10 C
−10 to −20 C
−20 to −30 C
−30 to −40 C
< −40 C
IR 9 Nov 1993 1830

Figure 9

SSM/I LWP 9 Nov 1993 1946 UTC

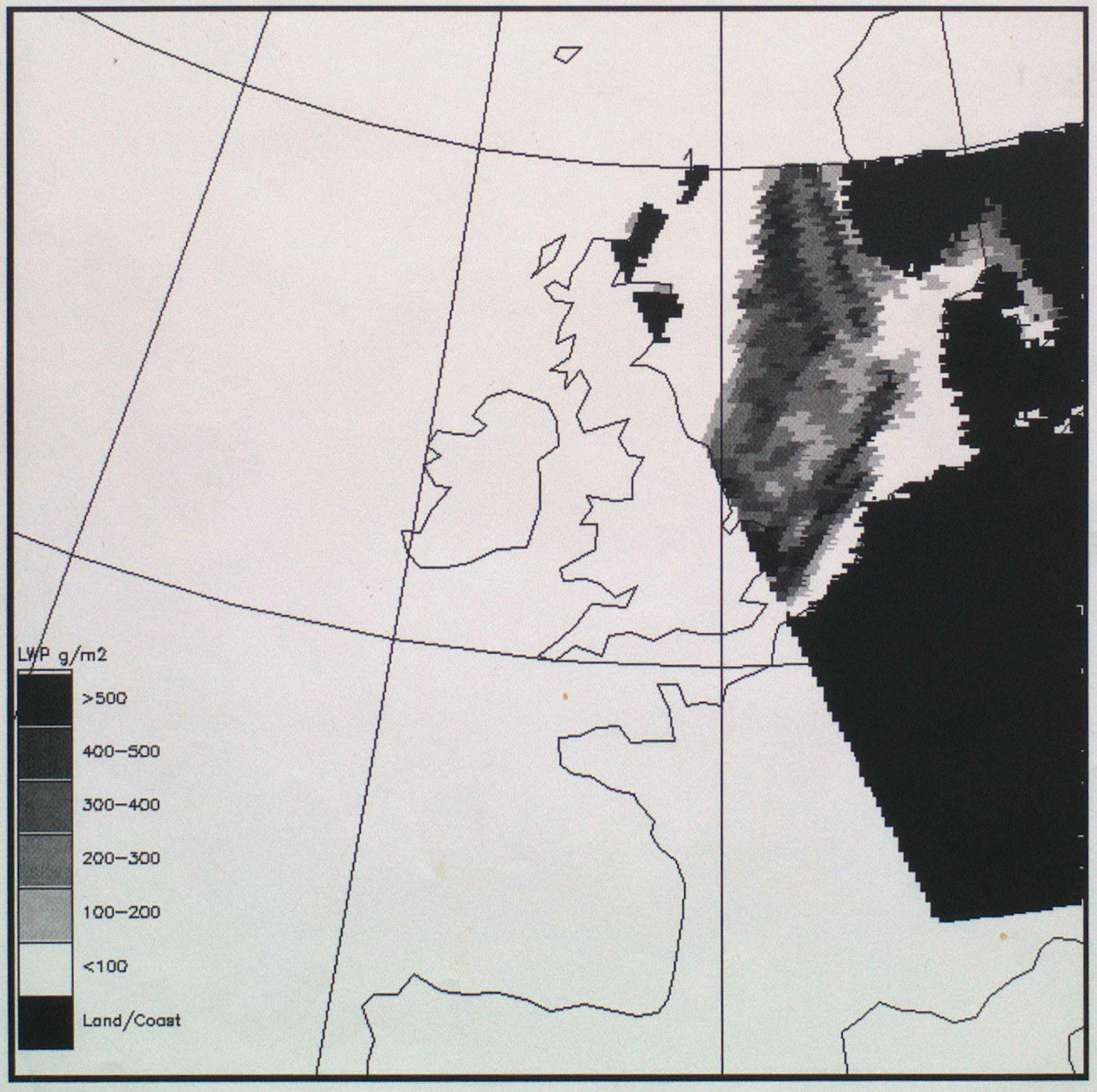

Figure 10

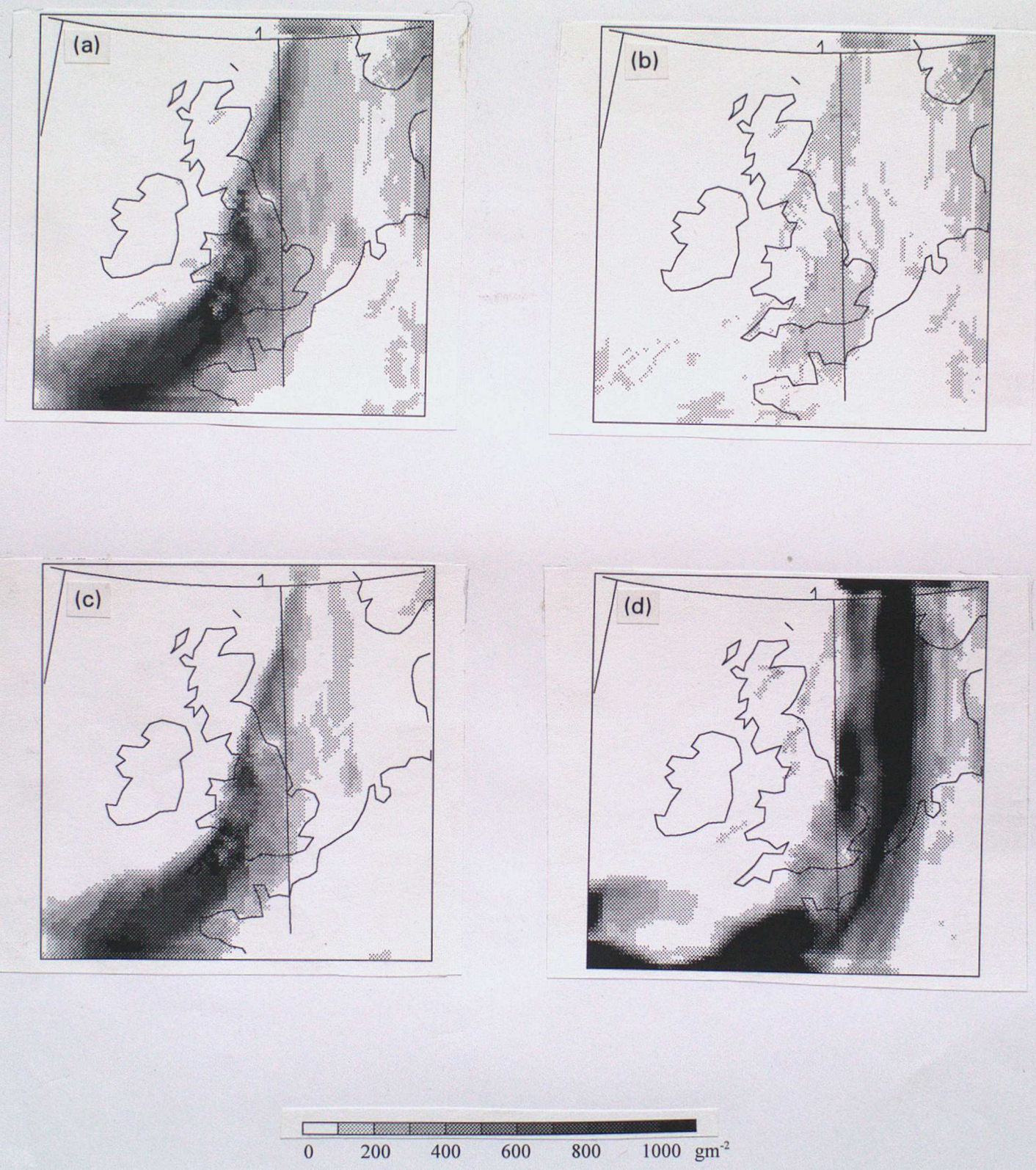

Figure 11

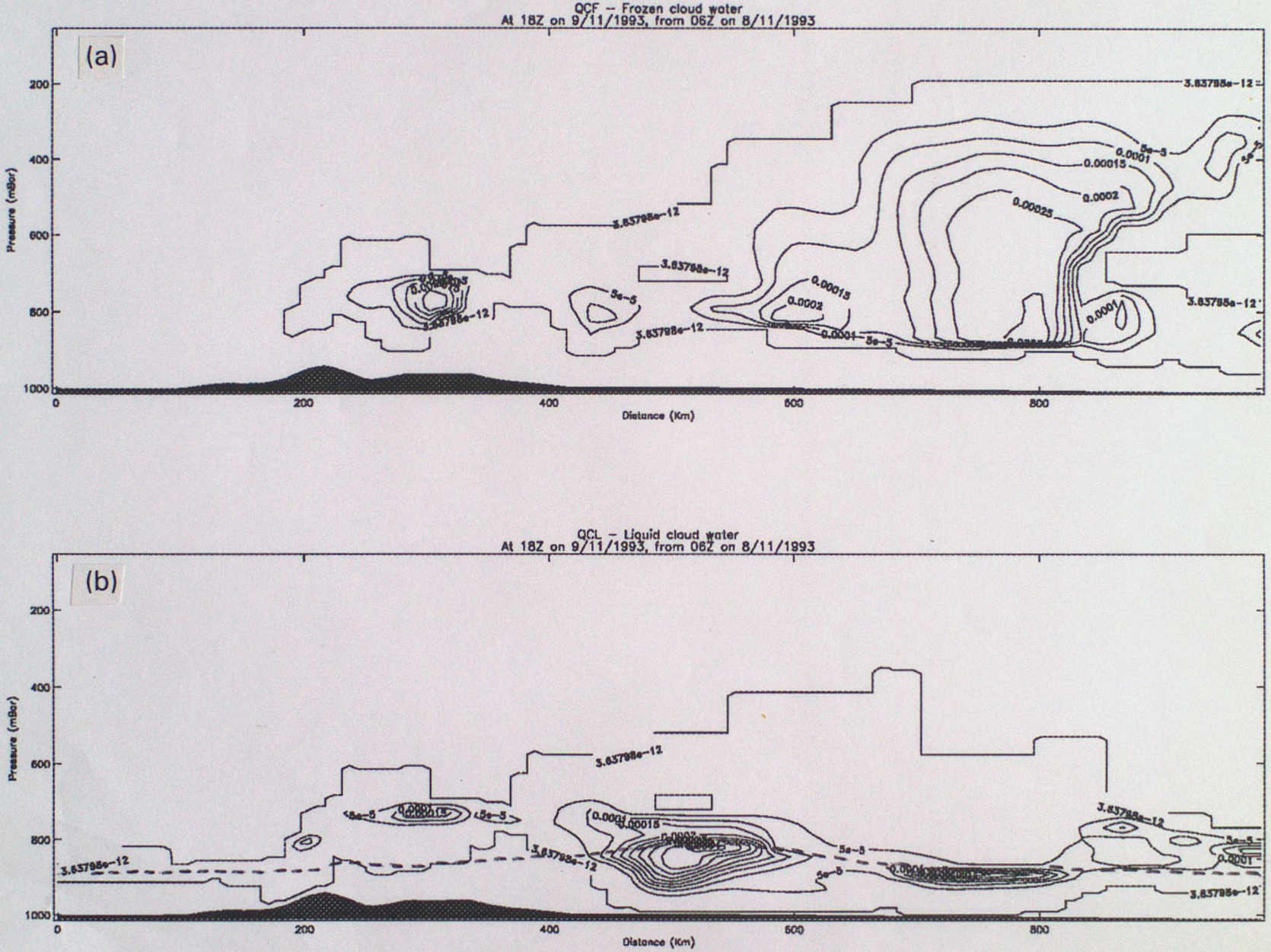
QCF -- Frozen cloud water
At 18Z on 9/11/1993, from 06Z on 8/11/1993
(a)
Pressure (mBar)
Distance (Km)
QCL -- Liquid cloud water
At 18Z on 9/11/1993, from 06Z on 8/11/1993
(b)
Pressure (mBar)
Distance (Km)

Figure 12

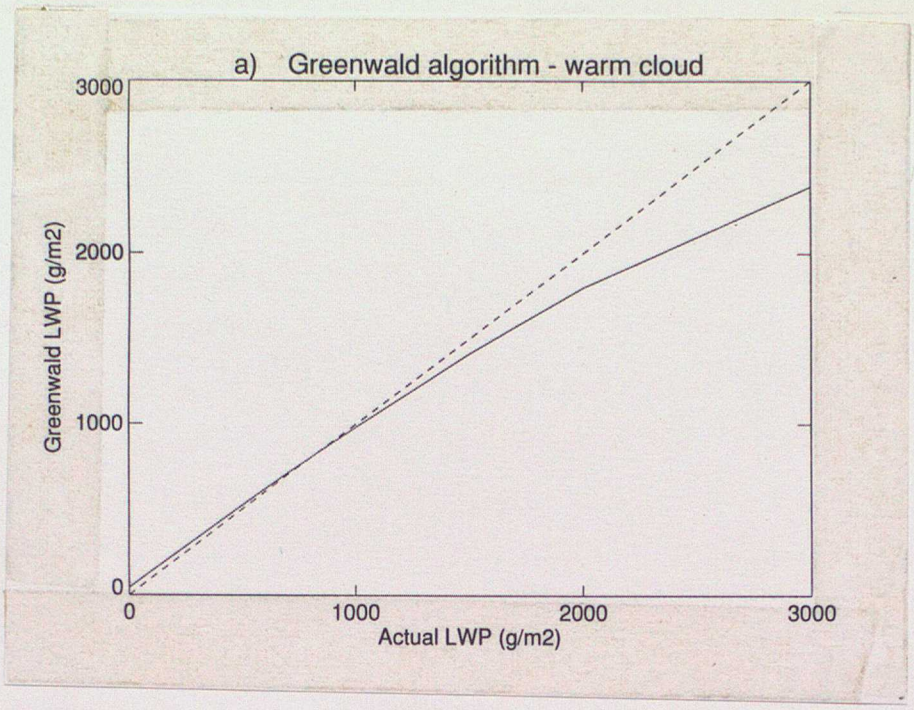
a) Greenwald algorithm - warm cloud
Greenwald LWP (g/m2)
3000
2000
1000
0
0
1000
2000
3000
Actual LWP (g/m2)

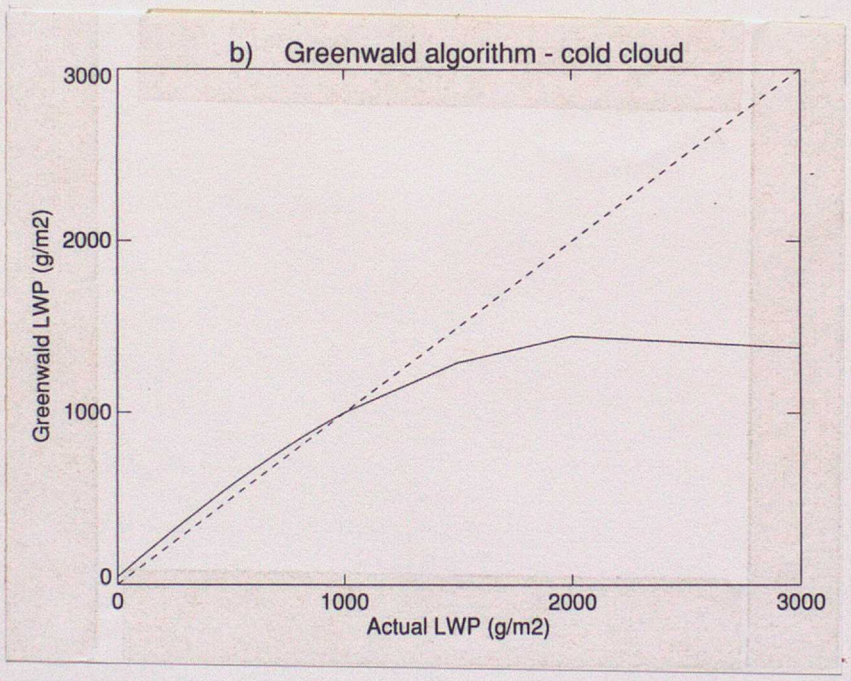
b) Greenwald algorithm - cold cloud
Greenwald LWP (g/m2)
3000
2000
1000
0
0
1000
2000
3000
Actual LWP (g/m2)

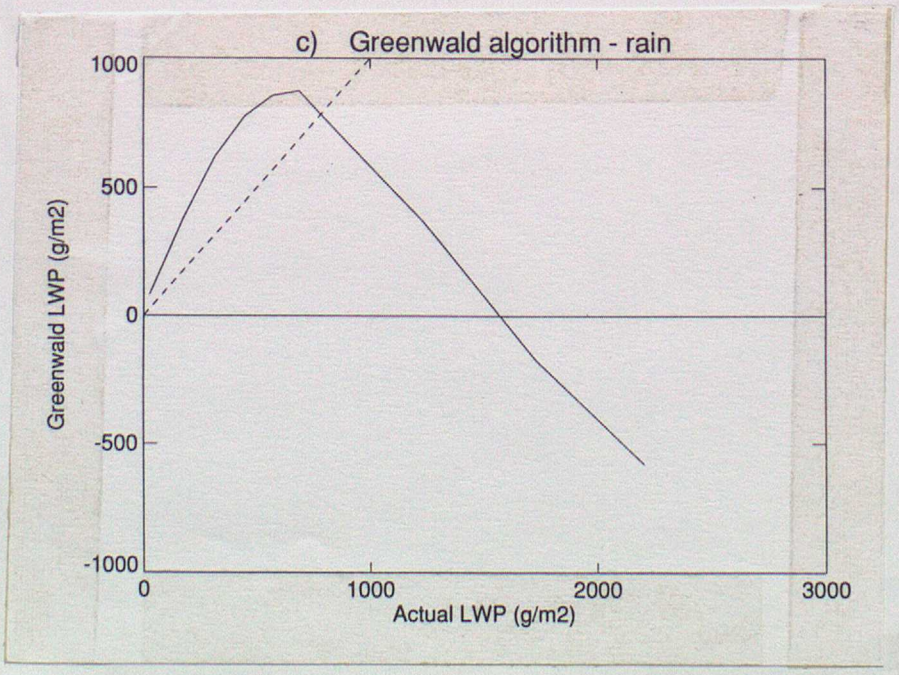
c) Greenwald algorithm - rain
Greenwald LWP (g/m2)
1000
500
0
-500
-1000
0
1000
2000
3000
Actual LWP (g/m2)

Figure 13

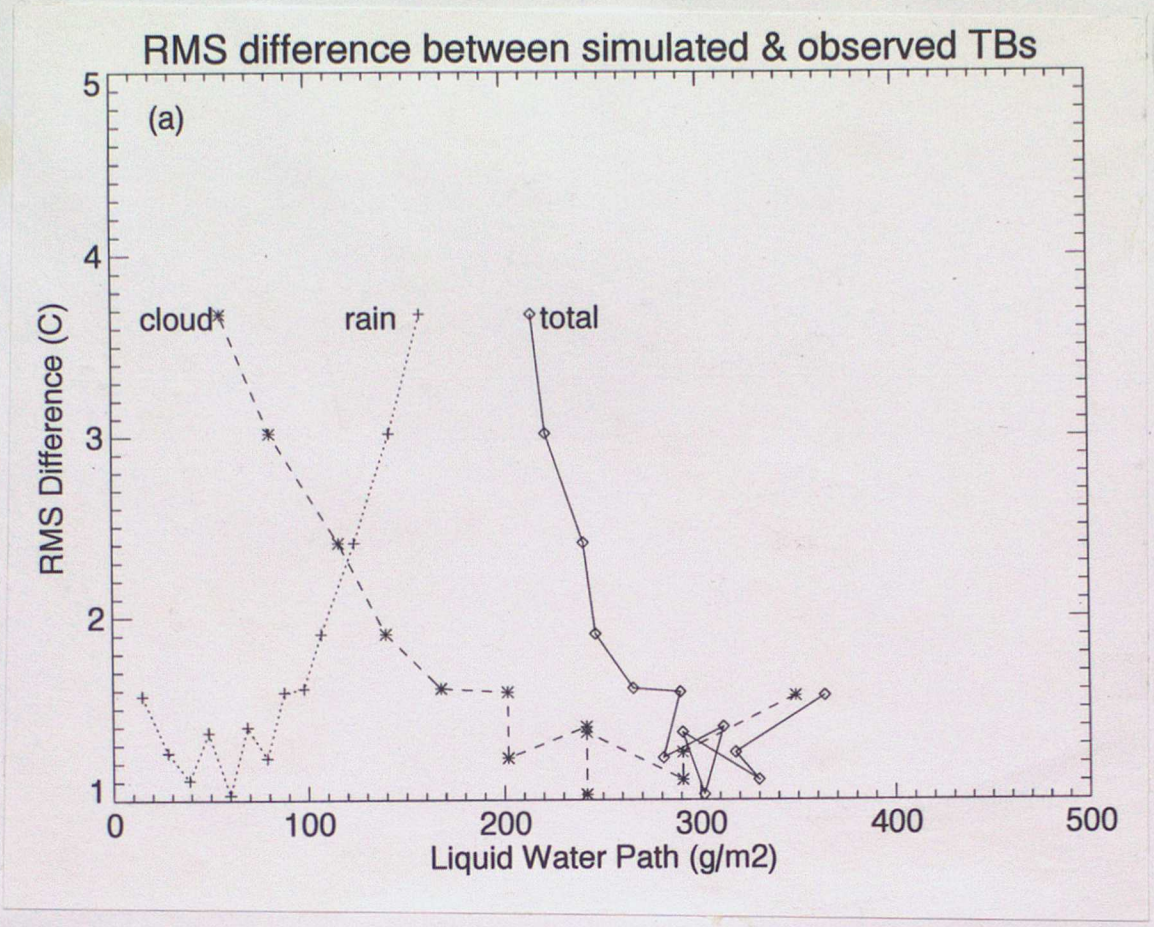
RMS difference between simulated & observed TBs
(a)
cloud
rain
total
RMS Difference (C)
Liquid Water Path (g/m2)
0
100
200
300
400
500
1
2
3
4
5

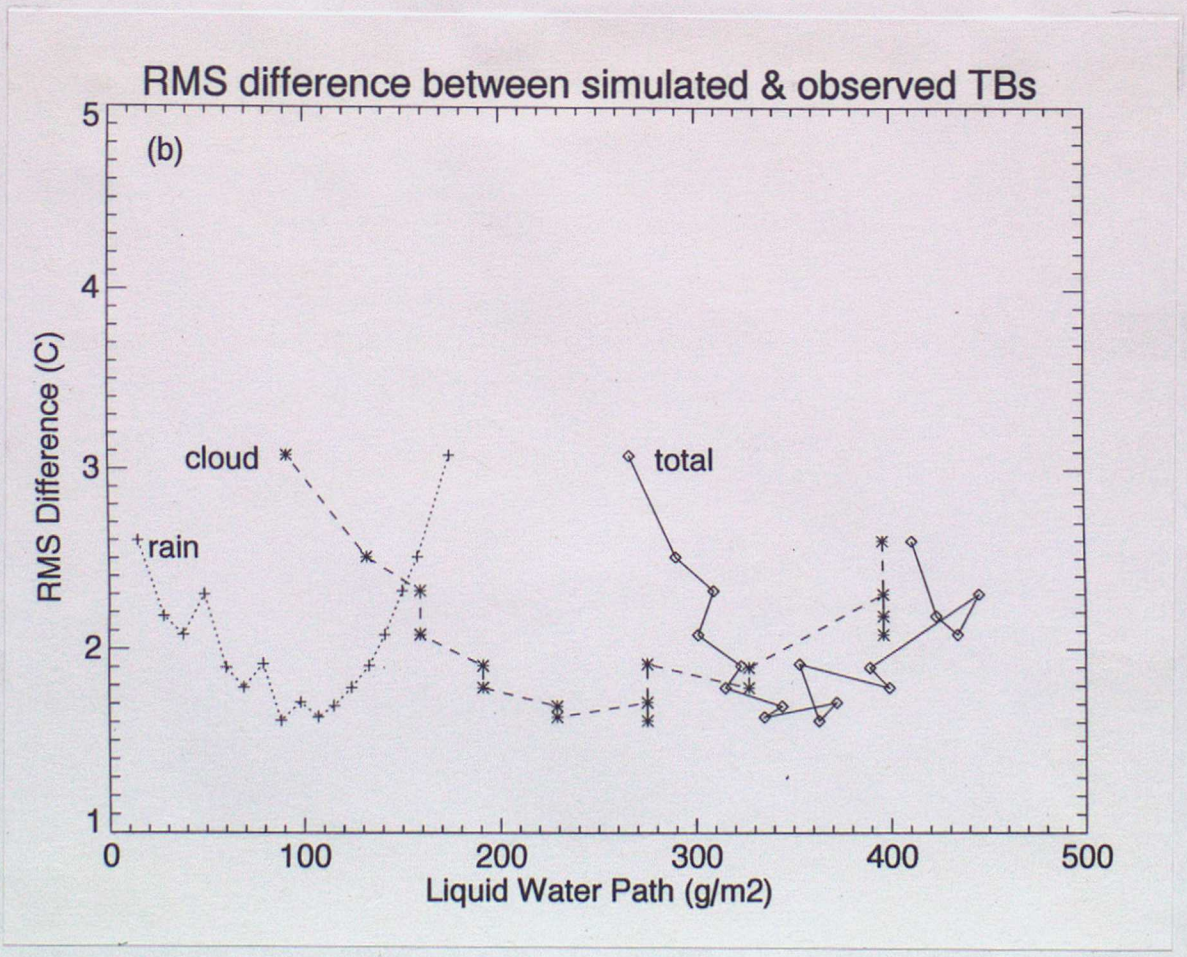
RMS difference between simulated & observed TBs
(b)
cloud
rain
total
RMS Difference (C)
Liquid Water Path (g/m2)
0
100
200
300
400
500
1
2
3
4
5